

## Real-time foul sewer hydraulic modelling driven by water consumption data from water distribution systems

Zhang, Qingzhou; Zheng, Feifei; Jia, Yueyi; Savic, Dragan; Kapelan, Zoran

**DOI**

[10.1016/j.watres.2020.116544](https://doi.org/10.1016/j.watres.2020.116544)

**Publication date**

2021

**Document Version**

Accepted author manuscript

**Published in**

Water Research

**Citation (APA)**

Zhang, Q., Zheng, F., Jia, Y., Savic, D., & Kapelan, Z. (2021). Real-time foul sewer hydraulic modelling driven by water consumption data from water distribution systems. *Water Research*, 188, 1-16. Article 116544. <https://doi.org/10.1016/j.watres.2020.116544>

**Important note**

To cite this publication, please use the final published version (if applicable). Please check the document version above.

**Copyright**

Other than for strictly personal use, it is not permitted to download, forward or distribute the text or part of it, without the consent of the author(s) and/or copyright holder(s), unless the work is under an open content license such as Creative Commons.

**Takedown policy**

Please contact us and provide details if you believe this document breaches copyrights. We will remove access to the work immediately and investigate your claim.

1 **Real-time foul sewer hydraulic modelling driven by water consumption data from water**  
2 **distribution systems**

3 Qingzhou Zhang<sup>1</sup>, Feifei Zheng<sup>2</sup>, Yueyi Jia<sup>3</sup>, Dragan Savic<sup>4</sup> and Zoran Kapelan<sup>5</sup>

4 <sup>1</sup>**Qingzhou Zhang:** Postdoctoral Research Fellow, College of Civil Engineering and  
5 Architecture, Zhejiang University, China. [wdswater@gmail.com](mailto:wdswater@gmail.com).

6 <sup>2</sup>**Feifei Zheng:** Corresponding author, Professor, College of Civil Engineering and  
7 Architecture, Zhejiang University, China. [feifeizheng@zju.edu.cn](mailto:feifeizheng@zju.edu.cn). Tel: +86-571-8820-6757.  
8 Postal address: A501, Anzhong Building, Zijingang Campus, Zhejiang University, 866  
9 Yuhangtang Rd, Hangzhou, China 310058.

10 <sup>3</sup>**Yueyi Jia:** PhD candidate, College of Civil Engineering and Architecture, Zhejiang  
11 University, China. [yueyi@zju.edu.cn](mailto:yueyi@zju.edu.cn).

12 <sup>4</sup>**Dragan Savic:** Chief Executive Officer, KWR Water Research Institute,  
13 [Dragan.Savic@kwrwater.nl](mailto:Dragan.Savic@kwrwater.nl), Professor, Centre for Water Systems, University of Exeter, North  
14 Park Road, Exeter, EX4 4QF, United Kingdom.

15 <sup>5</sup>**Zoran Kapelan:** Professor, Department of Water Management, Delft University of  
16 Technology, The Netherlands, [z.kapelan@tudelft.nl](mailto:z.kapelan@tudelft.nl)

17

18 **Abstract:** One way to address many issues (e.g., illicit inflows) within foul sewer systems  
19 (FSSs) is via real-time hydraulic models. However, a bottleneck within real-time FSS  
20 modelling is the lack of spatio-temporal manhole inflow data. To address this problem, this  
21 paper proposes a new method to develop real-time FSS models driven by water consumption  
22 data from associated water distribution systems (WDSs) that often have a proportionally  
23 larger number of sensors. Within the proposed method, the FSS manholes are integrated with  
24 the WDS water consumption nodes based on their underlying physical connections. An  
25 optimization approach is subsequently proposed to identify the transfer factor  $k$  between  
26 nodal water consumption and FSS manhole inflows based on historical observations. These  
27 identified  $k$  values combined with the acquired real-time nodal water consumption data from  
28 the WDS equipped with a dense network of sensors drive the FSS real-time modelling. The  
29 proposed method is applied to two real FSSs and results show that it can produce sewer flow  
30 and manhole water depth simulations matching well with observations at the monitoring  
31 locations with averaged  $R^2$ ,  $NSE$  and  $KGE$  (Kling-Gupta efficiency) around 0.99, 0.88 and  
32 0.92, respectively. It is anticipated that real-time models developed by the proposed method  
33 can be useful for the efficient FSS management and operation.

34 **Key words:** foul sewer system; water consumption data; real-time models; water distribution  
35 system

## 36 **1 Introduction**

37 Sewer networks are traditionally designed to collect wastewater from residential, commercial  
38 and/or industrial clients or possible stormwater from urban surfaces due to rainfall events.  
39 Collected wastewater is transported then downstream to wastewater treatment plants  
40 (WWTPs) or released directly into rivers (Bailey et al., 2019). These sewer networks are  
41 often called combined sewer systems (CSSs), which have been widely used in large cities  
42 around the world (Li et al., 2014). In recent years, there is a growing trend in separating CSSs  
43 into independent storm drainage systems and foul sewer systems (FSSs, Schilperoort et al.  
44 2013). The former are used to convey urban runoff solely to surface water bodies (e.g., rivers)  
45 and the latter deliver sewerage collected from houses and commercial buildings before being  
46 conveyed to treatment facilities. Such a separation is mainly driven by the purpose to  
47 improve urban water environments as combined sewer overflows (CSOs, Black and  
48 Endreny, 2006) would inevitably threaten the ecological health of the receiving water  
49 (Joseph-Duran et al., 2015).

50 Over the past decade, many FSSs around the world have experienced significant changes due  
51 to population growth and quick urbanization, which is especially the case in many developing  
52 countries such as China (Sweetapple et al., 2018). These changes are mainly represented by  
53 the expanded spatial scales of FSSs, the increased complexity in their topology structures and  
54 the aged systems (Rokstad and Ugarelli, 2015, Huang et al., 2018). This, consequently,  
55 results in significant challenges/difficulties for effective FSS management and operation, and  
56 hence many issues exist (Garda et al., 2016). A typical issue is the deposits in the FSSs,

57 including sediments (Seco et al., 2018), fat, oil and grease (FOG, Liu et al., 2016) and toilet  
58 papers (Eren and Karadagli, 2012). All those deposits can directly affect flow capacity of the  
59 sewers, causing overflows from CSOs and manholes as well as potential water quality issues  
60 (e.g, odor issues, Liu et al., 2016; Talaiekhosani et al., 2016). Another common issue is the  
61 illicit discharges from local factories (Irvine et al. 2011; Banik et al. 2017), where these  
62 discharges often contain toxic substances (e.g., heavy metals) that are often beyond the  
63 processing capacity of the downstream WWTPs. This, therefore, can result in functional  
64 failures of WWTPs and consequently significant contamination of the receiving water body  
65 (McCall et al. 2016). In addition to issues of deposits and illicit discharges, leaks of the  
66 sewers, groundwater infiltration and illicit connections between FSSs and stormwater pipes  
67 are frequently reported, inducing serious contamination to the surrounding water  
68 environments (Lepot et al., 2017; Beheshti and Saegrov, 2019).

69 The issues mentioned above have appreciably affected the urban water environments due to  
70 the resultant overflows from CSOs/manholes and leaks of FSSs. One way to address these  
71 issues is the placement of sensors within the FSS to monitor the water depths and sewer flows,  
72 thereby triggering a warning when the observations are significantly higher or lower than the  
73 historical data (Ahm et al. 2016). However, due to the high purchase cost and intensive  
74 maintenance efforts associated with these sensors, the monitoring network is often sparse for  
75 the majority of the FSSs (Kleidorfer et al., 2012). Consequently, a warning associated with  
76 the potential issues (e.g., overflows or leaks) can be only available for the very limited  
77 number of FSS locations in the proximity of sensors. In addition, the abnormal observations  
78 at the monitoring locations may be caused by sudden discharges increases caused by the

79 water users, rather than the illicit discharges, resulting in a potentially high likelihood of false  
80 warning (Koch et al. 2011). More importantly, relying solely on the observations from the  
81 sewer sensors cannot offer predictions on the hydraulic status of the entire FSS in future  
82 (Bruen and Yang, 2006). To this end, real-time sewer hydraulic modelling can be promising  
83 in addressing the issues associated with the FSSs as mentioned above, where the hydraulic  
84 variables such as water depths and sewer flows across the entire FSS are simulated in  
85 real-time. These simulations, combined with observations at the monitoring locations, can be  
86 used to deduce whether leaks, illicit discharges, deposits and illicit connections exist in the  
87 FSS, as well as facilitate the localization of such events.

88 Manhole inflow data (i.e., sewer discharges of the water users) at a high time resolution (say  
89 every 30 minutes) is the key to enable the development of a real-time FSS hydraulic model.  
90 However, discharge data of such a high temporal and spatial resolution are typically  
91 unavailable in engineering practice, resulting in a large challenge for real-time modeling of  
92 FSS (Breinholt et al., 2013). To deal with this problem, a widely used approach is to calibrate  
93 a model to estimate manhole inflows with the aid of limited in-sewer observations (Korving  
94 and Clemens, 2005). While some calibration methods are available in the literature (e.g., di  
95 Pierro et al., 2005, Khu et al., 2006, Broekhuizen et al., 2020), they mainly focus on  
96 calibrating the underlying rainfall-runoff relationship for the combined sewer systems in an  
97 off-line manner, thereby predicting the floods or sewer overflows caused by rainfall. These  
98 previously published methods, therefore, cannot be used or at least are difficult to estimate  
99 FSS manhole inflows in real-time.

100 The real-time management of the FSS has received great attention over the past few decades,  
101 with the main focus on system real-time control based on observations (Schütze et al., 2002;  
102 Sara et al., 2020). More specifically, real-time control is defined as a timely operation of an  
103 FSS based on continuously monitored process data. Those data are water levels and sewer  
104 flows in the system, with operations including the activation of pumps, sluice gates and weirs  
105 used to improve system performance (e.g., reduce the overflows, Schütze et al., 2003).  
106 However, these real-time control studies operated the hydraulic facilities (e.g., pumps) with  
107 the aid of system observations rather than FSS simulations, and hence they differ  
108 significantly from the real-time FSS hydraulic modelling, which is the aim of the present  
109 study.

110 The main difficulty associated with the calibration of FSS manhole inflows based on the  
111 limited number of monitoring sites is the “equifinality” (Khu et al., 2006). More specifically,  
112 a large number of manhole inflow combinations can produce similar agreements between  
113 simulated and observed water levels at monitoring locations. As a result, it is very difficult, if  
114 not impossible, to identify a particular parameter set (i.e., manhole inflow combination) that  
115 can represent the true underlying spatial distribution of the discharges from water users into  
116 the FSS.

117 To address the “equifinality” issue, this paper proposes a new method to enable the  
118 development of real-time FSS hydraulic model. Within the proposed method, the FSS model  
119 is integrated with its corresponding water distribution system (WDS) hydraulic model for the  
120 same area being considered. Such a model integration approach is possible as the WDS

121 models have already been widely used (Walski et al., 2003). In addition, the number of  
122 sensors (e.g., smart demand meters, pressure sensors and flow meters) deployed in the WDSs  
123 can be large, which is, at least partly, driven by the quick developments of the Internet of  
124 Things in recent years (Zheng et al., 2018). Such a dense sensor network can greatly facilitate  
125 the estimation of real-time nodal water consumption for the WDS models as demonstrated in  
126 previous studies (Creaco et al., 2019). This is especially the case in recent years as smart  
127 demand meters have been increasingly used in many WDSs, providing water consumption  
128 data for many users (not only large users but also residential users) in a real-time manner  
129 (typically every 15 or 30 minutes, Creaco et al., 2018). Such near real-time and high-density  
130 spatial water consumption data can be assimilated with the limited in-sewer observations to  
131 develop a real-time FSS hydraulic model. This is the key feature and novelty of the method  
132 presented in this paper.

133 The concept of incorporating water consumption data into FSS modeling can be dated back to  
134 Bruke et al. (1986), where an FSS model was calibrated using monthly water use records.  
135 More recently, Bailey et al. (2019) presented a new FSS model, where the stochastically  
136 simulated water demands were imported into the sewer network model. While these limited  
137 previous studies have made great contributions in assimilating water use records into FSS  
138 modelling (mainly used for FSS design purpose), the water consumption data used are either  
139 collected manually at a very low time resolution (e.g., monthly, Bruke et al., 1986) or  
140 provided by a stochastic simulator (Bailey et al., 2019). Consequently, these data cannot  
141 represent the true underlying temporal and spatial variations of the manhole inflows.  
142 Therefore, they cannot be used to develop real-time FSS models, which is the focus of this



143 study.

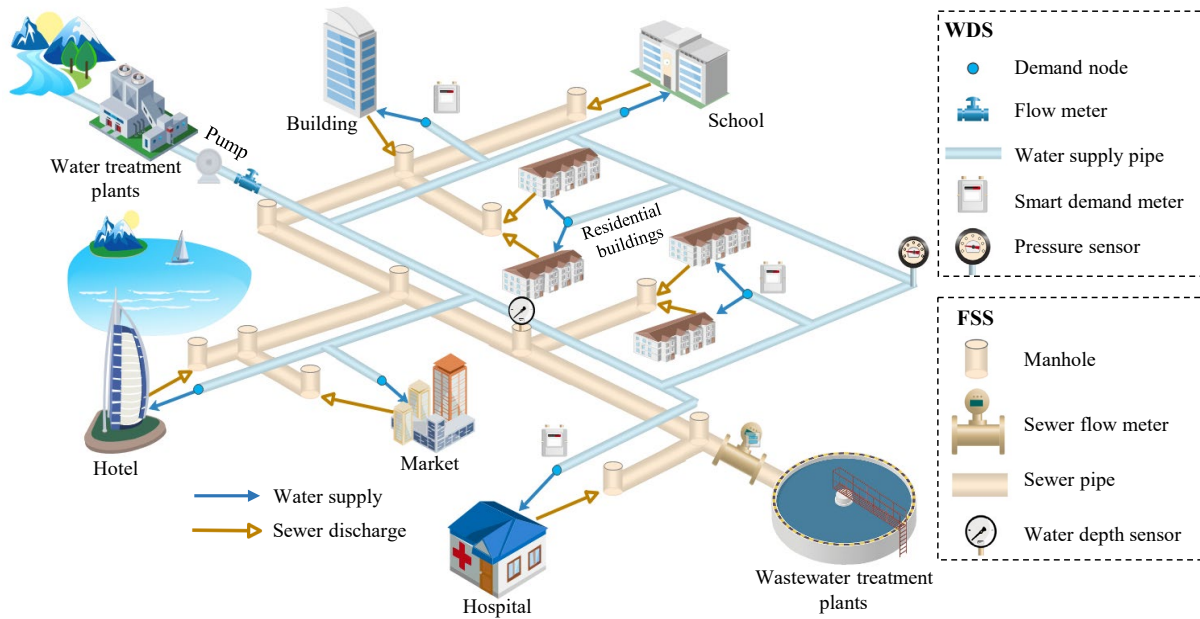
144 The key feature of the proposed method is that the real-time FSS model is developed using a  
145 large number of existing sensors within the WDSs. This implies that it is not necessary to  
146 deploy a large number of sewer sensors (which is often very expensive in terms of both  
147 sensor purchases and maintenance) to enable real-time sewer modelling, making the proposed  
148 method attractive for practical applications. This paper is organized as follows. The proposed  
149 methodology is described in Section 2, followed by the descriptions of the case studies  
150 considered in Section 3. Results and discussions are given in Section 4. Finally, the conclusion  
151 section (Section 5) shows the main observations and implications of this paper.

## 152 **2. Methodology**

### 153 **2.1 The overall modelling concept**

154 Fig.1 illustrates the overall concept of the proposed method, where a foul sewer system (FSS)  
155 and a water distribution system (WDS) for a small area are presented. Typically, raw water  
156 from reservoirs or rivers is pumped into the water treatment plants in order to improve water  
157 quality to a required standard (Wu et al., 2011). Subsequently, the treated water is conveyed  
158 to the WDS, satisfying demands for various users including residents, schools, hospitals,  
159 industrial and commercial buildings, as shown in Figure 1. To ensure water supply safety,  
160 sensors are often deployed in the WDS (Figure 1), including pressure sensors, flow meters  
161 and smart demand meters. The latter have been increasingly being deployed in recent years to  
162 monitor water consumptions for the users in a near real-time manner (Creaco et al., 2018).

163 Consequently, such a dense sensor network enables the development of real-time WDS  
 164 modelling, which has been an important trend within the water supply domain (both research  
 165 and industry) due to its great merits in facilitating effective system management as  
 166 highlighted in Creaco et al. (2019).



167

168 **Fig. 1 An illustration of the concept for the proposed modelling method, where a water**  
 169 **distribution system and a foul sewer system are presented**

170 Inherently, local residents or commercial/industrial users discharge sewage after water  
 171 consumption as illustrated in Figure 1. Sewer pipes collect and convey the sewage to  
 172 downstream wastewater treatment plants, with a limited number of water depth or sewer flow  
 173 sensors installed to monitor hydraulic state of the system. Consequently, the following  
 174 equation can be used to represent the underlying relationship between water consumption and  
 175 sewage discharge for user  $i$ :

176 
$$d_i = F(q_i, k_i, t_i) \tag{1}$$

177 where  $d_i$  is the sewer discharge rate of user  $i$  (i.e., manhole inflow rate) resulting from its  
178 water consumption  $q_i$  taken from the WDS,  $t_i$  represents the time delay, i.e., the time  
179 between the clean water entering the user property and the time it reaches the local sewer  
180 network,  $k_i$  is the transfer factor for user  $i$ , representing the proportion of supplied water  
181 that ends up in the local sewer network;  $k_i$  typically has a value between 0.7 and 1.0  
182 (Behzadian and Kapelan 2015). Equation (1) represents the fundamental rule/assumption in  
183 the proposed method used to build the connections between the WDS water consumption  
184 data and the FSS manhole inflows.

185 Fig.2 presents the overall methodology of the proposed method, with two modules involved.  
186 The first module consists of three phases, which are carried only once in an offline manner,  
187 and the second module only has the fourth phase (Phase 4) of the proposed method, which  
188 runs in real-time. The details are given below.

189 *Phase 1: Integrate the WDS and FSS models (carry out once).* Within this phase, the  
190 FSS and WDS models are developed with hydraulic facility information (e.g., water supply  
191 pipes, tanks, sewer pipes) taken from external sources such as the GIS or asset management  
192 system. This is followed by the building of the connections between each WDS demand node  
193 and the FSS manhole based on the spatial distance with details given in Section 2.2.

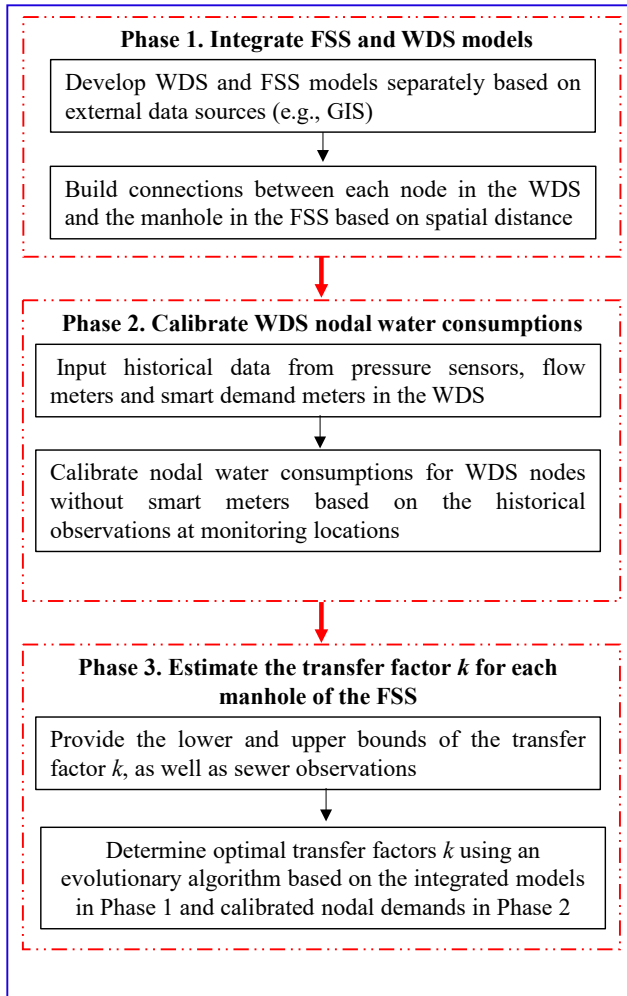
194 *Phase 2: Calibrate nodal water consumptions of the WDS.* It should be highlighted that  
195 the calibration of the nodal water consumptions in Phase 2 is conducted offline, which is used  
196 to provide data for Phase 3. More specifically, Based on a particular time period of historical

197 data from pressures sensors, flow meters and smart demand meters deployed in the WDS, the  
198 nodal water consumption without smart demand meters are estimated for a given time  
199 resolution (often equals the time resolution of the flow or pressure sensors) with details given  
200 in Section 2.3

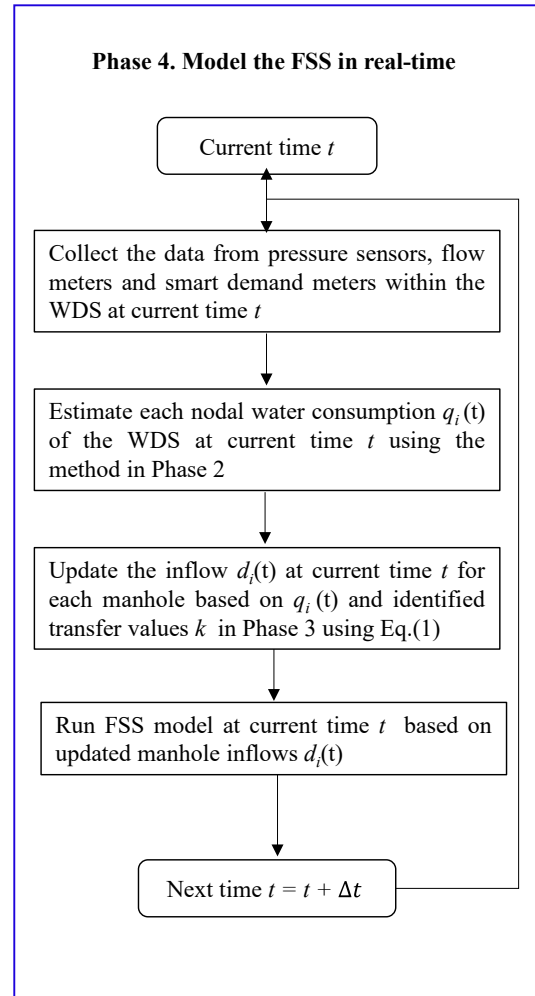
201 *Phase 3: Estimate the transfer factor  $k$  for each manhole of the FSS.* According to the  
202 identified relationship between WDS nodes and the FSS manholes in Phase 1, as well as the  
203 calibrated nodal water consumptions in Phase 2, the transfer factor  $k$  is determined. For this,  
204 an evolutionary algorithm (EA) is applied with the objective function defined in Eq. (9-13)  
205 and using sewer observations, with details given in Section 2.4.

206 *Phase 4: Model the FSS in a real-time manner.* Data from pressure sensors, flow meters  
207 and the available smart demand meters in the WDS are acquired at the current time  $t$ . These  
208 data are used as the inputs for the real-time WDS modelling to estimate water consumption  
209 for each node ( $q_i$ ) within the WDS (Section 2.3). Eq. (1) is subsequently used to update the  
210 manhole inflows  $d_i$  based on the known  $q_i$  and identified  $k$  values (Phase 3). Finally, the FSS  
211 is modelled by updating manhole inflows  $d_i$  in real-time. This offers short-term hydraulic  
212 predictions (water depths at manholes and flow rates in sewer pipes) of the entire FSS with a  
213 particular time resolution (if say every 30 minutes used in this paper).

### Offline module (carry out once)



### Real-time module



214

215

**Fig. 2 The overall methodology of the proposed method**

216 It is noted that a few assumptions are made in the proposed method, with the justification  
217 given below.

218 (i) Given that the proposed FSS real-time modelling method is driven by water  
219 consumption data from the WDS, the number of available smart demand meters in the WDS  
220 is important to ensure the high accuracy of the FSS simulations. For the two case studies  
221 considered in this paper, the number of smart demand meters is reasonably high, making  
222 them perfectly suited for the demonstration of the proposed method. However, some WDSs

223 may have relatively low coverage of the smart demand meters (e.g., only installed for large  
224 demand users). While such a case would not affect the application of the proposed method,  
225 the accuracy of the WDS nodal water consumption values and the FSS real-time simulations  
226 can be affected. However, it is anticipated that smart demand meters are increasingly used by  
227 water utilities as a result of the quick developments in the Internet of Things (Zheng et al.,  
228 2018; Creaco et al., 2019), and hence the applicability of the proposed method is only going  
229 to grow.

230 (ii) The proposed method assumes that observations from the WDS and FSS sensors  
231 (including smart demand meters) are accurate within the applications in this study. However,  
232 in reality, observation errors can exist due to the sensor malfunctions or signal transmission  
233 issues. Therefore, it is necessary to incorporate the potential observation errors into the  
234 modelling framework. Although that is an important study direction, it is beyond the scope of  
235 the paper and will be the focus of future work.

236 (iii) As shown in Equation (1), the time  $t_i$  implies that the nodal water  
237 consumption  $q_i$  estimated at time  $t$  using the smart demand meter or the real-time  
238 calibration method (section 2.3) should correspond to the manhole inflow at time  $t + t_i$ . The  
239 value of  $t_i$  can be dependent on the particular user properties, including the characteristics  
240 of the water supply area associated with the demand node, as well as the physical  
241 characteristics (e.g., length and slopes) of the connecting sewer pipes between users and the  
242 corresponding manholes. In this study,  $t_i$  is ignored as this value is typically small, ranging  
243 from several minutes up to 15 minutes for many cases (Wu et al., 2011). This assumption is  
244 considered valid in our study as the time resolution used for real-time FSS modelling in this

245 paper is lower (i.e., 30 minutes).

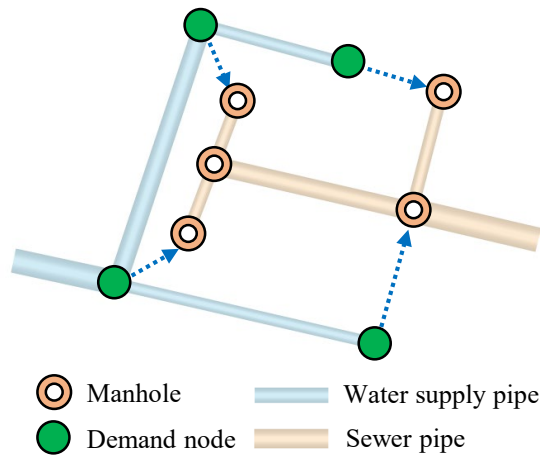
246 (iv) In this study, a linear transfer function with a constant factor of  $k$  is proposed to  
247 describe the underlying relationship between the nodal water consumption and manhole  
248 inflows. While being simple in practical implementation, the transfer function as well as the  $k$   
249 factor can be affected by not only the time delay  $t_i$  in Equation (1), but also the infiltration  
250 inflows and the properties of water users. More specifically, the transfer function may be  
251 different between the water users with or without smart demand sensors, and the  $k$  factor may  
252 temporally vary, or even change as a function of different water users. These influences need  
253 further consideration in future study along this research line.

## 254 **2.2 Integrate the FSS and WDS models**

255 Typically, FSS and WDS models are developed with the aid of the geographic information  
256 system (GIS) or the asset management system for the analyzed area (Behzadian and Kapelan,  
257 2015; Huang et al., 2018). The details (e.g., locations and length) of various system  
258 components including pipes, tanks, valves and pumps can be taken from the GIS. This is  
259 often followed by system skeletonization in which many facilities (mainly small pipes) are  
260 removed or simplified without significantly affecting the hydraulic properties of the original  
261 full system (Huang et al., 2020). To enable the practical application of Eq. (1), it is important  
262 to build the connection between each demand node  $i$ , representing the water consumption in  
263 the WDS model, and the manhole, representing the facility to collect the sewages in the FSS  
264 model. Such a connection indicates that the consumption at the demand node  $i$  is received by  
265 its associated manhole. To this end, the WDS and FSS models are integrated within their  
266 development processes in this study.

267 Figure 3 illustrates the proposed integration method, where a water demand node in the WDS  
268 model is assigned to the manhole of the FSS model within a shortest distance from each other.  
269 The rationale behind this is that manholes are often built near the water users (nodes in the  
270 WDS model) to collect their sewerage discharges. Consequently, two cases are available as  
271 shown in Figure 3, which are (i) one demand node is assigned to a manhole, and (ii) multiple  
272 demand nodes are assigned to a single manhole. In addition to these two relatively simple  
273 cases, in practice, one demand node can be associated with multiple manholes, which is  
274 possible when this demand node represents many users. However, it is difficult to know the  
275 proportion of the total discharge associated with each relevant manhole. For the sake of  
276 simplicity, a single manhole with the minimum spatial distance to this demand node is  
277 selected to deliver the total discharge. While such a simplification can cause an unrealistic  
278 hydraulic status in a very small area relative to the original full system, its impacts on the  
279 overall results can be negligible. Since each demand node (say node  $i$ ) in the WDS is  
280 assigned to a particular manhole in the FSS model, the water consumption of this node ( $q_i$ ) is  
281 considered as the approximate manhole inflows ( $d_i$ ). Their underlying flow relationship  
282 needs to be further accurately determined with the incorporation of the transfer factor  $k_i$  as  
283 shown in Equation (1).





284

285 **Fig. 3 Illustration of the proposed integration method for FSS and WDS model**

286 **developments**

287 It is noted that when a higher level of accuracy is needed for a practical application,  
 288 individual water consumption and sewer connections could be identified if required. This will  
 289 lead to a slight modification on the WDS and FSS model topologies, which can better reflect  
 290 the flows of supplied drinking water and generated wastewater by different users.

291 **2.3 Calibrate nodal water consumption based on historical observations**

292 Based on the built connections between each WDS node and its corresponding FSS manhole  
 293 as described in Section 2.2, nodal water consumption is the driver for triggering the real-time  
 294 FSS modelling. In the WDSs, many smart demand meters can be available, providing near  
 295 real-time water consumption data (if say every 15 minutes or 30 minutes) for WDS nodes  
 296 (users), especially for water users with large demand. However, in practice, it may not be  
 297 necessary to have smart meters installed at each demand node, and hence this study adopts a  
 298 calibration method to enable the estimation of water consumption at the nodes without smart

299 demand meters.

300 In this study, the numerical approach described in Zhang et al. (2018) is selected to calibrate  
301 the nodal water consumptions due to its demonstrated efficiency. The objective function of  
302 this adopted numerical method is formulated as the weighted sum of squared differences  
303 between the field-observed and model-simulated responses (pressures and flows) at  
304 monitoring points in the WDS within a particular time period (i.e., the time resolution of the  
305 monitoring data), i.e. as follows:

$$306 \quad \text{Min} : f(\mathbf{q}) = \sum_{i=1}^{NH} w_h^i [H_i^o - H_i(\mathbf{q})]^2 + \sum_{j=1}^{NF} w_q^j [Q_j^o - Q_j(\mathbf{q})]^2 = \begin{bmatrix} \mathbf{H}^o - \mathbf{H}(\mathbf{q}) \\ \mathbf{Q}^o - \mathbf{Q}(\mathbf{q}) \end{bmatrix}^T \mathbf{W} \begin{bmatrix} \mathbf{H}^o - \mathbf{H}(\mathbf{q}) \\ \mathbf{Q}^o - \mathbf{Q}(\mathbf{q}) \end{bmatrix} \quad (2)$$

307 where  $\mathbf{q}$  is the vector of nodal water consumptions in the WDS, including known water  
308 consumption data at nodes with smart demand meters and unknown nodal water consumption  
309 data;  $NH$  and  $NF$  are the numbers of observed nodal pressures and pipe flows, respectively;  
310  $w_h^i$  and  $w_q^j$  are the weighting factors for observed pressures at the  $i^{th}$  node and observed  
311 flows at the  $j^{th}$  pipe, respectively, where  $w_h^i = 1/(H_i^o)^2$  and  $w_q^j = 1/(Q_j^o)^2$  are used in this  
312 study following Kun et al. (2015) and Zhang et al. (2018).  $H_i^o$  and  $H_i(\mathbf{q})$  are the observed  
313 and simulated pressures at the  $i^{th}$  node respectively;  $Q_j^o$  and  $Q_j(\mathbf{q})$  are the observed and  
314 simulated flows at the  $j^{th}$  pipe respectively. Equation (2) can be expressed in the matrix  
315 form (see above) by using  $\mathbf{H}^o = [H_1^o, H_2^o, \dots, H_{NH}^o]^T$ ,  $\mathbf{Q}^o = [Q_1^o, Q_2^o, \dots, Q_{NF}^o]^T$ ,  
316  $\mathbf{H}(\mathbf{q}) = [H_1(\mathbf{q}), H_2(\mathbf{q}), \dots, H_{NH}(\mathbf{q})]^T$ ,  $\mathbf{Q}(\mathbf{q}) = [Q_1(\mathbf{q}), Q_2(\mathbf{q}), \dots, Q_{NF}(\mathbf{q})]^T$ , and  
317  $\mathbf{W} = \text{diag}([w_h^1, w_h^2, \dots, w_h^{NH}, w_q^1, w_q^2, \dots, w_q^{NF}])$ .

318 Expanding Eq. (2) through the first-order Taylor series:

319 
$$f(\mathbf{q} + \Delta\mathbf{q}) \approx \begin{bmatrix} \Delta\mathbf{H} - \mathbf{J}_H \Delta\mathbf{q} \\ \Delta\mathbf{Q} - \mathbf{J}_Q \Delta\mathbf{q} \end{bmatrix}^T \mathbf{W} \begin{bmatrix} \Delta\mathbf{H} - \mathbf{J}_H \Delta\mathbf{q} \\ \Delta\mathbf{Q} - \mathbf{J}_Q \Delta\mathbf{q} \end{bmatrix} \quad (3)$$

320 where  $\Delta\mathbf{H} = \mathbf{H}^o - \mathbf{H}(\mathbf{q})$  and  $\Delta\mathbf{Q} = \mathbf{Q}^o - \mathbf{Q}(\mathbf{q})$  are the differences between the observed and

321 simulated values of nodal pressures and pipe flows, respectively;  $\mathbf{J}_H = \frac{\partial \mathbf{H}(\mathbf{q})}{\partial \mathbf{q}}$  and

322  $\mathbf{J}_Q = \frac{\partial \mathbf{Q}(\mathbf{q})}{\partial \mathbf{q}}$  are the Jacobian matrix with details given in Zhang et al. (2018). Since Eq. (2)

323 is a convex function (Kun et al., 2015), the minimum objective value of Eq. (2) can be

324 obtained when its first-order derivative (Eq. (3)) equals to zero, that is:

325 
$$\frac{df(\mathbf{q} + \Delta\mathbf{q})}{d\Delta\mathbf{q}} = -2 \begin{bmatrix} \mathbf{J}_H \\ \mathbf{J}_Q \end{bmatrix}^T \mathbf{W} \begin{bmatrix} \Delta\mathbf{H} - \mathbf{J}_H \Delta\mathbf{q} \\ \Delta\mathbf{Q} - \mathbf{J}_Q \Delta\mathbf{q} \end{bmatrix} = 0 \quad (4)$$

326 By solving Eq. (4),  $\Delta\mathbf{q}$  can be obtained as follows:

327 
$$\Delta\mathbf{q} = \left( \begin{bmatrix} \mathbf{J}_H \\ \mathbf{J}_Q \end{bmatrix}^T \mathbf{W} \begin{bmatrix} \mathbf{J}_H \\ \mathbf{J}_Q \end{bmatrix} \right)^{-1} \begin{bmatrix} \mathbf{J}_H \\ \mathbf{J}_Q \end{bmatrix}^T \mathbf{W} \begin{bmatrix} \Delta\mathbf{H} \\ \Delta\mathbf{Q} \end{bmatrix} \quad (5)$$

328 
$$\mathbf{q}^{s+1} = \mathbf{q}^s + \Delta\mathbf{q}^s \quad (6)$$

329 where  $s = 0, 1, \dots, S$  is the iteration number ( $S$  is the maximum allowed number of

330 iterations). It is highlighted that the water consumption at nodes with smart demand meters

331 are known within the entire calibration process and hence  $\Delta\mathbf{q}$  is only considered for the

332 nodes without smart meters. To ensure the estimated nodal water consumption values are

333 practically meaningful, the domain knowledge has been incorporated within the calibration

334 process in this study as shown below (Wu et al., 2010):

335 
$$q_i^{s+1} = \begin{cases} q_i^{\min}, & \text{if } q_i^{s+1} < q_i^{\min} \\ q_i^{\max}, & \text{if } q_i^{s+1} > q_i^{\max} \\ q_i^{s+1}, & \text{others} \end{cases} \quad (7)$$

336 where  $q_i^{\min} = (1-p) \times q_i^{\text{initial}}$  and  $q_i^{\max} = (1+p) \times q_i^{\text{initial}}$  are the minimum and maximum  
 337 allowed water consumptions at node  $i$  respectively;  $p$  is the percentage generally within  
 338 10%~20% in practice (Zhang et al., 2018);  $q_i^{\text{initial}}$  is estimated using

339 
$$q_i^{\text{initial}} = \frac{l_i}{L_T - L_M} (Q_T - Q_M) \quad (8)$$

340 where  $l_i$  is the length of the pipe associated with node  $i$ ;  $L_T$  and  $L_M$  is the total pipe  
 341 length of all nodes and the length of pipes associated with smart demand meters respectively;  
 342  $Q_T$  is the total water consumption of the WDS at a given time period (e.g., 30 minutes),  
 343 which is estimated based on the flow meters installed at the outlet of the water treatment  
 344 plants and volume changes in the tanks if available;  $Q_M$  is the sum of the water  
 345 consumption values measured by the available smart demand meters within the WDS at a  
 346 given time period.

347 The calibration process at each time period (i.e., the time resolution of the monitoring data,  
 348 e.g. 30 minutes) is executed by iteratively updating  $\Delta \mathbf{q}$  in Eq. (6) until the maximum value  
 349 of vector  $\|\Delta \mathbf{q}\|$  is smaller than a given threshold value  $\varepsilon$  (e.g.  $\varepsilon = 0.1$ ). The entire  
 350 calibration process is executed again once the monitoring data from sensors are updated,  
 351 representing a real-time hydraulic calibration for the WDS. It is noted that the pipe resistance  
 352 coefficients are not calibrated in a real-time manner as these values are not likely to change

353 over a short time period (Kun et al., 2016).

#### 354 **2.4 Estimate the transfer factor $k$ for each FSS manhole**

355 As stated in Eq. (1), the nodal consumption data determined in Section 2.3 ( $q_i$ ) cannot be  
356 directly taken as the manhole inflows ( $d_i$ ) due to the inevitable loss during the transporting  
357 process within the facilities of the users (Behzadian and Kapelan, 2015). In this study, a  
358 transfer factor  $k_i$  is used to represent the proportion of water consumption used by node  $i$   
359 that has been collected by its corresponding manhole. Such a factor can vary as a function of  
360 the properties of the water users, such as user types (commercial users or common resident  
361 users) and habits of water usages (Bailey et al., 2019). Therefore, the transfer factor needs to  
362 be calibrated for each demand node based on the nodal water consumption data and the sewer  
363 observations (e.g., sewer flow rates or water depth in the manholes) in the FSS. In this study,  
364 the transfer factor  $k_i$  associated with each demand node is considered to be approximately  
365 constant over time because the user properties are overall constant over a short time period  
366 (Bailey et al., 2019).

367 To calibrate the transfer factor  $\mathbf{K} = [k_1, k_2, \dots, k_n]^T$  of the entire FSS with a total of  $n$   
368 manholes with external inflows, the following objective function is defined,

$$\text{Min} : F(\mathbf{K}) = \sum_{t=T_w}^T \left( \sum_{i=1}^M [g(h_i^o(t)) - g(h_i^s(t))]^2 + \sum_{j=1}^N [g(f_j^o(t)) - g(f_j^s(t))]^2 \right) \quad (9)$$

$$[\mathbf{h}_i^s, \mathbf{f}_j^s] = [h_i^s(t_1), h_i^s(t_2), \dots, h_i^s(T); f_j^s(t_1), f_j^s(t_2), \dots, f_j^s(T)] = F_s(\mathbf{D}(T)) \quad (10)$$

$$\mathbf{D}(T) = \begin{bmatrix} d_1(t_1), d_2(t_1), \dots, d_n(t_1) \\ d_1(t_2), d_2(t_2), \dots, d_n(t_2) \\ \dots \\ d_1(T), d_2(T), \dots, d_n(T) \end{bmatrix} \quad (11)$$

$$d_i(t) = k_i \times q_i(t) \quad (12)$$

$$k_i^{\min} \leq k_i \leq k_i^{\max}, \quad i = 1, 2, \dots, n \quad (13)$$

369 where  $T$  is the time period with observations used for FSS calibration;  $T_w$  is the  
 370 warming-up time period for model setting up (Guo et al., 2020);  $M$  and  $N$  are the numbers of  
 371 observed water depths at the manholes and flow rates in the sewer pipes, respectively;  $h_i^o(t)$   
 372 and  $f_j^o(t)$  are observed water depth at manhole  $i$  and observed flow rate at sewer pipe  $j$  at  
 373 time  $t$  respectively;  $h_i^s(t)$  and  $f_j^s(t)$  are simulated water depth at manhole  $i$  and simulated  
 374 flow rate at sewer pipe  $j$  at time  $t$  respectively;  $g()$  is a linear function used to convert water  
 375 depths and pipe flow rates into the same scale, thereby enabling both terms in the right side of  
 376 Eq. (9) are approximately equivalent in terms of the objective function value.

377  $\mathbf{h}_i^s = [h_i^s(t_1), h_i^s(t_2), \dots, h_i^s(T)]$  is a vector representing the simulated water depths of manhole  $i$   
 378 over the entire time period of  $T$ ;  $\mathbf{f}_j^s = [f_j^s(t_1), f_j^s(t_2), \dots, f_j^s(T)]$  is a vector representing the  
 379 simulated sewer flow rates of pipe  $j$  over the entire time period of  $T$ ;  $\mathbf{D}(T)$  is a  $T \times n$   
 380 matrix, representing the inflows of all manholes across the total time period of  $T$ . The values  
 381 of  $\mathbf{h}_i^s$  and  $\mathbf{f}_i^s$  are computed using  $F_s(\mathbf{D}(T))$  as shown in Eq. (11). In this study a  
 382 simulation package called Storm Water Management Model (SWMM, Rossman, 2010) is  
 383 employed to calculate  $\mathbf{h}_i^s$  and  $\mathbf{f}_i^s$ . In Eq. (12),  $d_i(t)$  is the inflow rate of manhole  $i$  at time  
 384  $t$ , and  $q_i(t)$  is the water consumption of node  $i$  at time  $t$  determined by real-time WDS

385 modelling as described in Section 2.3.  $k_i^{\min}$  and  $k_i^{\max}$  are the minimum and maximum  
386 allowable values of  $k_i$ , which can be determined by engineering experience. In this study,  
387  $k_i^{\min} = 0.7$  is used for each demand node of the WDS, and  $k_i^{\max} = 1.0$  is used for each WDS  
388 node with smart demand meters, but  $k_i^{\max} = 1.3$  is used for WDS nodes without smart meters.  
389 This is because water consumptions of nodes without smart meters are calibrated using the  
390 method described in Section 2.3, and hence the identified values can inevitably deviate from  
391 the true water consumption values at a certain extent. To mitigate this potential impact, the  
392 maximum value of the transfer factor for these nodes is increased to 1.3. In this paper, an  
393 evolutionary algorithm (EA, Zheng et al., 2017) combined with the SWMM package is  
394 employed to solve the optimization problem defined in Eq. (9-13). While different EAs are  
395 available in literature, Borg (Hadka and Reed, 2013) is used in this study due to its  
396 well-demonstrated performance in dealing with complex water resources optimization  
397 problems, with more algorithm details in Section 3.2.

398 In the proposed FSS calibration method, manhole inflows are considered as the only  
399 calibration parameters due to their large temporal and spatial variations, with which the  
400 transfer factor  $k$  for each manhole can be estimated. It should be noted that Manning's  
401 roughness coefficients of the sewer pipes can also affect the hydraulics of the FSS. However,  
402 previous studies have shown that the impacts of the small to moderate variation in Manning's  
403 roughness coefficients of sewer pipes are limited (Rossman and Huber, 2017). In addition, the  
404 physical pipe properties (e.g., pipe ages and materials) that affect the Manning's roughness  
405 coefficient are unlikely to vary in a short time period (Zhang et al., 2018) and hence it is not  
406 considered within the real-time FSS modelling. It is highlighted that the values of

407  $\mathbf{K} = [k_1, k_2, \dots, k_n]^T$  are calibrated using a particular time period of historical water  
408 consumption data and in-sewer observations in an offline manner (carried out once as shown  
409 in Figure 2).

## 410 **2.5 Model the FSS in real-time**

411 It is noted that Phases 1-3 in Sections 2.2-2.4 are carried offline (in the offline module as  
412 shown in Figure 2), aimed to identify the transfer factors between the WDS nodal water  
413 consumptions and the FSS manhole inflows. This is followed by the real-time FSS modelling  
414 (real-time module of the proposed method in Figure 2) with the following steps.

415 **Step 1:** Collect the data from pressure sensors, flow meters and the available smart demand  
416 meters in the WDS at current time  $t$ ,

417 **Step 2:** Estimate the water consumption for each WDS node without smart demand meters,  
418  $q_i(t)$  in Equation (1), using the method described in Section 2.3 (Phase 2) based on the  
419 observations from Step 1.

420 **Step 3:** Update the manhole inflow  $d_i(t)$  based on  $q_i(t)$  and the identified transfer factor  $k$  in  
421 Phase 3 of the offline module using Equation (1).

422 **Step 4:** Run the FSS hydraulic model based on the manhole inflow  $d_i(t)$ , producing the water  
423 depths and sewer flows for the entire FSS within the time resolutions (30 minutes in this  
424 study). This is followed by moving to Step 1 at  $t = t + \Delta t$  where  $\Delta t$  is the time resolution  
425 of the FSS modelling ( $\Delta t = 30$  minutes in this study).

## 426 **2.6 Metrics used for performance evaluation**



427 Five statistical metrics are used in this paper to evaluate the performance of the proposed  
 428 method in simulating the FSS hydraulic variables. They are the absolute percentage error  
 429 (*APE*), the mean absolute percentage error (*MAPE*), the coefficient of determination ( $R^2$ ), the  
 430 Nash-Sutcliffe model efficiency (*NSE*), and the Kling-Gupta Efficiency (*KGE*). These five  
 431 metrics are selected due to their wide applications in assessing the model performance within  
 432 the water resources domain (Mu et al., 2020). The *APE* between the  $i^{th}$  observation  $Y_i$  and  
 433 its corresponding simulation  $\hat{Y}_i$  is defined as

$$434 \quad APE = \left| \frac{Y_i - \hat{Y}_i}{Y_i} \right| \times 100\% \quad (14)$$

$$435 \quad MAPE = \frac{1}{n} \sum_{i=1}^n \left| \frac{Y_i - \hat{Y}_i}{Y_i} \right| \times 100\% \quad (15)$$

436 where  $n$  is the total number of data points. As shown in Eq. (14) and (15), a lower value of  
 437 *APE* or *MAPE* indicate an overall better model performance. The  $R^2$  is a goodness-of-fit  
 438 measure for linear regression models, which can be mathematically described as (Gujarati et  
 439 al., 2009):

$$440 \quad R^2 = \frac{\left( \sum_{i=1}^n (Y_i - \tilde{Y})(Y_i - \bar{Y}) \right)^2}{\sum_{i=1}^n (Y_i - \tilde{Y})^2 \sum_{i=1}^n (Y_i - \bar{Y})^2} \quad (16)$$

441 where  $\bar{Y}$  represents the mean of the observations and  $\tilde{Y}$  is the mean of the simulations. A  
 442 large value of  $R^2$  represents a better model performance. The *NSE* is defined as follows  
 443 (Nash and Sutcliffe, 1970), with a larger value implying a better model performance:

444

$$NSE = 1 - \frac{\sum_{i=1}^n (Y_i - \hat{Y}_i)^2}{\sum_{i=1}^n (Y_i - \bar{Y})^2} \quad (17)$$

445 The *KGE* metric is mathematically described as follows (Knoben et al., 2019):

446

$$KGE = 1 - \sqrt{(r-1)^2 + \left(\frac{\sigma_{sim}}{\sigma_{obs}} - 1\right)^2 + \left(\frac{\mu_{sim}}{\mu_{obs}} - 1\right)^2} \quad (18)$$

447 where  $r$  is the linear correlation between observations and simulations;  $\sigma_{sim}$  and  $\sigma_{obs}$  are  
 448 the standard deviation in simulations and observations, respectively;  $\mu_{sim}$  and  $\mu_{obs}$  are the  
 449 mean of simulations and observations, respectively. A large value of *KGE* means that the  
 450 simulations can match observations better, with  $KGE=1$  representing the best model  
 451 performance.

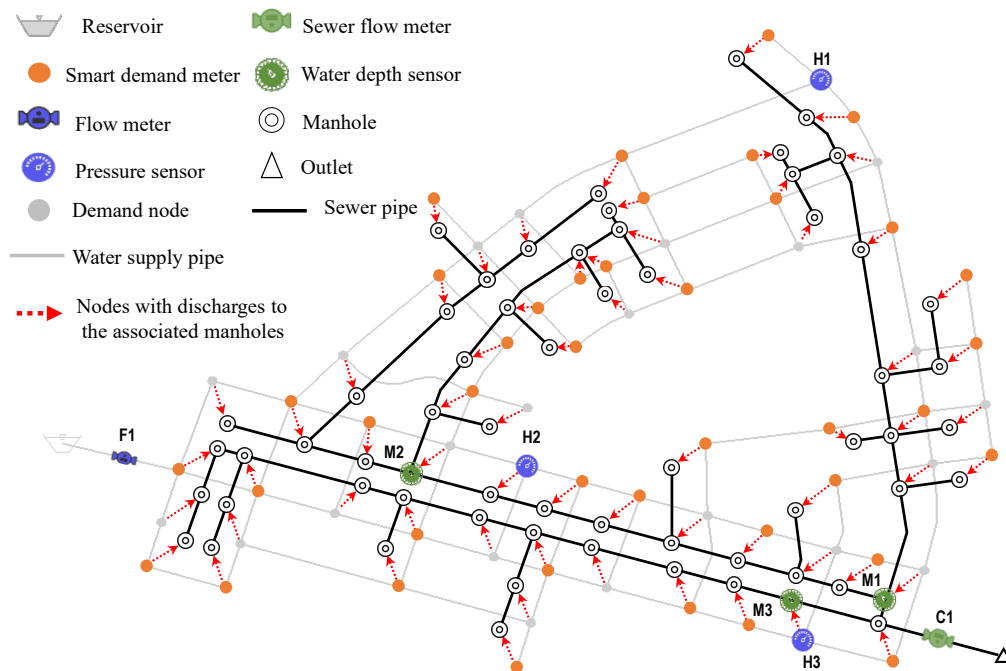
### 452 3. Case studies

#### 453 3.1 Case study description

454 Two real-world FSSs in China, the Benk network (BKN) and the Xiuzhou network (XZN),  
 455 are selected as case studies to demonstrate the utility of the proposed method. These two  
 456 FSSs are selected as their associated WDSs have good coverage of monitoring sensors,  
 457 especially the smart demand meters. In addition, BKN and XZN respectively represent scales  
 458 of a relatively small region and a town, aimed to demonstrate the utility of the proposed  
 459 method in handling the FSSs with different complexity levels.

460 BKN consists of one outlet, 64 manholes and 64 sewer pipes (Figure 4), delivering the

461 wastewater for the users with water supplied by a WDS (referred to as WDS-BNK).  
 462 WDS-BNK is composed of one reservoir, 65 nodes and 93 pipes, as well as one flow meter,  
 463 three pressure sensors and 40 smart water demand meters (Figure 4), providing  
 464 approximately 4,800 m<sup>3</sup> of water per day. As shown in Figure 4, one in-sewer flow meter and  
 465 three water depth sensors with a 30-minute time resolution have been installed in BKN, with  
 466 an average discharge of about 4,100 m<sup>3</sup>/day. The dotted arrow lines in Figure 4 represent the  
 467 receiving manhole for each demand node determined based on the spatial distances.  
 468 Observations from the WDS-BNK and BNK sensors are recorded for consecutive 31 days  
 469 without rainfall or snowfall events in winter with a 30-minute time resolution.



470

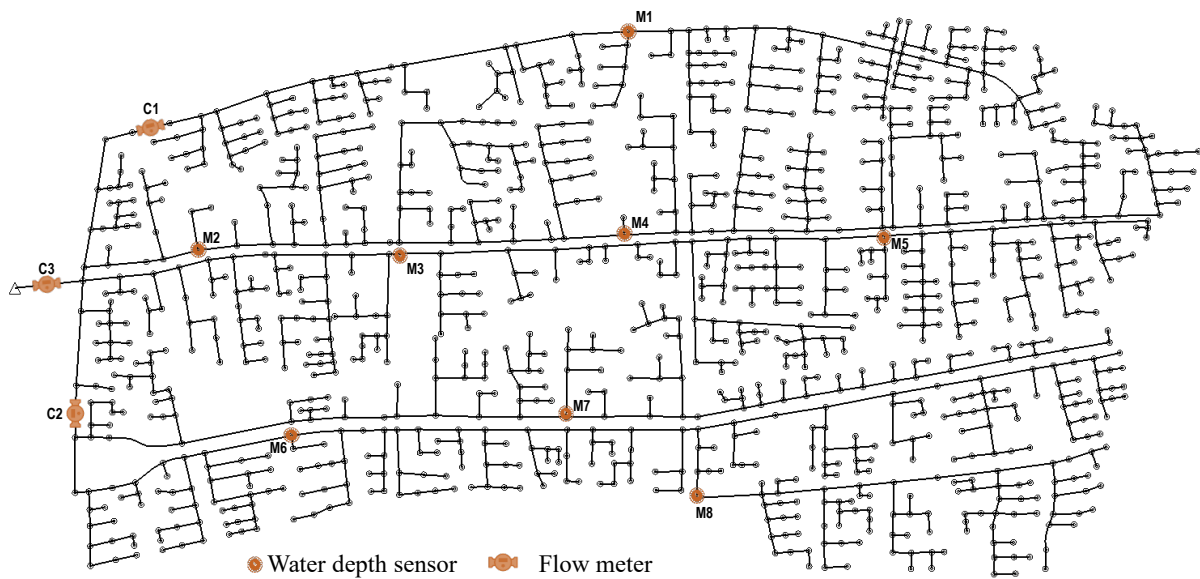
471 **Fig. 4 The layout and sensor locations of the BKN case study and its corresponding**

472

**WDS-BNK**

473 The XZN system is a large-scale complex FSS in Jiaying City, with a total length of  
 474 approximately 86 km and an average discharge of about 21,500 m<sup>3</sup>/day. The layout of the

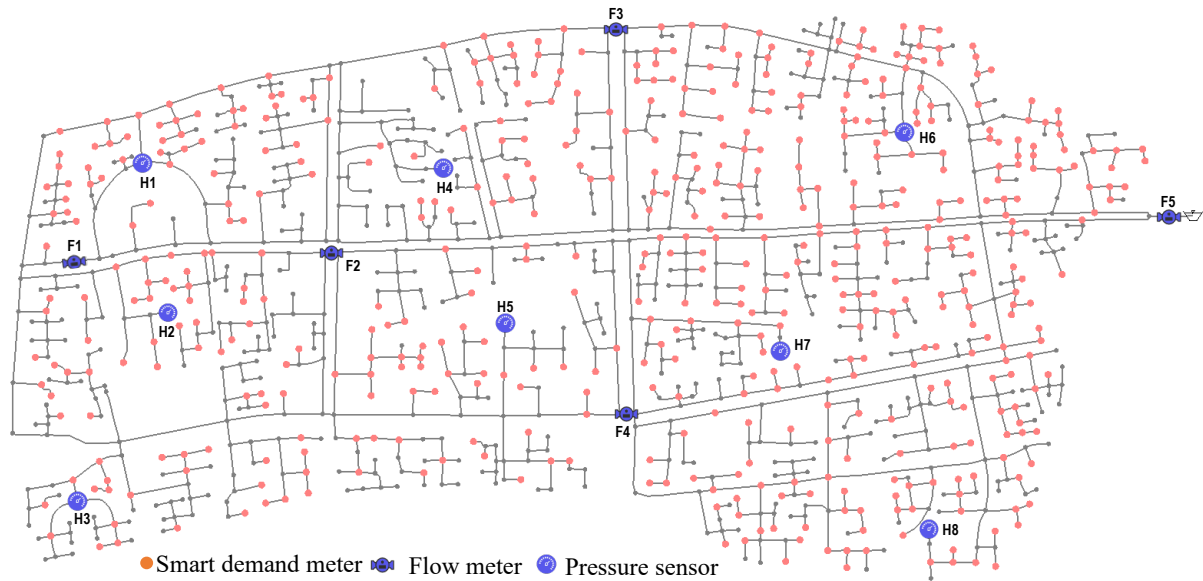
475 XZN network is shown in Fig. 5, consisting of one outlet, 1,214 manholes and 1,214 sewer  
476 pipes. As shown in Fig. 5, three flow meters and eight water depth sensors have been  
477 installed in this FSS. The WDS that supplies water demands for this area (referred as  
478 WDS-XZN) has one reservoir, one pump station, 1,119 nodes and 1,137 water consumption  
479 pipes as shown in Fig. 6. In the WDS-XZN network, five flow meters, eight pressure sensors  
480 and 525 smart demand meters are deployed as illustrated in Fig. 6. The WDS-XZN network  
481 supplies approximately 23,150 m<sup>3</sup> per day for a population about 107,500 living in this area  
482 within the Jiaxing City. As the same for the BKN network, the data from the WDS-XZN and  
483 XZN sensors are recorded for consecutive 31 days without rainfall or snowfall events in  
484 winter with a 30-minute time resolution.



485

486

**Fig. 5 The layout and sensor locations of the XZN case study**



487

488

**Fig. 6 The layout and sensor locations of the WDS-XZN**

489

### **3.2 Implementation of the proposed method**

490

The EPANET2.0 and SWMM5.1 (Rossman, 2000, 2010) were used as WDS and FSS

491

hydraulic simulation model respectively in this study. For both case studies, historical data of

492

the first 17 consecutive days from WDS sensors with a 30-minute time resolution were used

493

to estimate the water consumptions of nodes without smart meters. This led to a total of 816

494

( $17 \times 24 \times 2$ ) time periods with nodal water consumptions to be calibrated for each WDS.

495

These estimated nodal water consumption data were subsequently used to identify the

496

transfer factors  $k$  of the FSS based on sewer observations at the first 17 days.

497

The WDS and FSS sewer observations of the remaining 14 days ( $14 \times 24 \times 2$  data points used

498

for model validation) were used to run the real-time FSS models with a 30-minute time

499

resolution. In other words, the first set of WDS observations at the validation period (the last

500

14 days) was considered as the observations at time  $t$  in the real-time module of Figure 2 ( $\Delta t$

501 =30 minutes), followed by the execution of the four steps in Section 2.5.

502 For the nodal water consumption calibration, the termination error was set as  
503  $\max(\|\Delta\mathbf{q}\|) \leq 0.1$  (Eq. 6), the maximum allowed iterations was  $S=100$  (Eq. 6), and the  
504 adjustment range of nodal water consumptions was  $p=20\%$  for each WDS (Eq. 7). For the  
505 WDS-BNK (Figure 4), observations of the first 17 days from two pressure sensors (H1 and  
506 H3) and the flow meter F1 were used for calibration, and the records of pressure sensor H2  
507 were used for validation. For the WDS-XZN (Figure 6), observations of the first 17 days  
508 from H1, H3, H4, H6 and H8 pressure sensors, as well as F2, F3, F4 and F5 flow meters were  
509 utilized for model calibration, and the records of H2, H5, H7 and F1 were used for validation.  
510 The first three days were considered as the warming-up time period for the FSS model setting  
511 up as stated in Eq. (9), i.e.,  $T_w=3$  days. The observations of the next 14 days were used for  
512 FSS model calibration, and the remaining observations of 14 days were utilized for validating  
513 the performance of the real-time FSS models. The linear scale function  $g()$  in Eq. (9) for  
514 each case study is defined as

$$515 \quad g(x) = \frac{x - x_{\min}}{x_{\max} - x_{\min}} \quad (17)$$

516 where  $x$  represents the observed or simulated values at monitoring points;  $x_{\min}$  and  $x_{\max}$   
517 are the lower and upper bounds, respectively. These two parameters for each monitoring point  
518 are determined by analyzing historical observation data over 14 days (i.e., the calibration time  
519 period) in this paper.

520 The evolutionary algorithm Borg (Hadka and Reed, 2013) was selected to solve the proposed

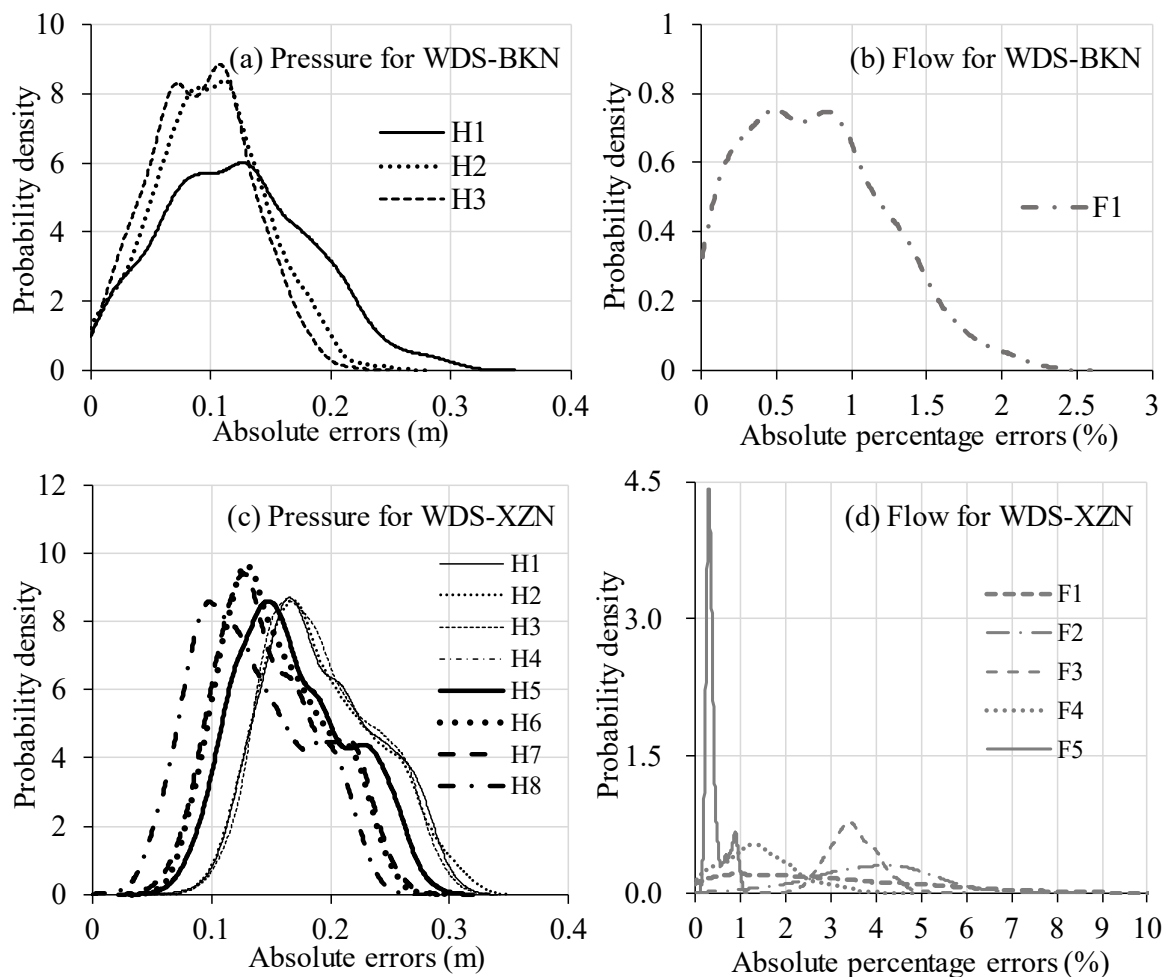
521 calibration problem defined in Eq. (9-13) due to its great performance in handling complex  
522 urban water resources and engineering optimization problems (Reed et al., 2013, Zheng et al.,  
523 2016). The initial population size of Borg applied to BKN and XZN case studies were 500  
524 and 1,000 respectively, and the maximum allowable iterations are 50,000 for both case  
525 studies. The default values of the other parameters of Borg were used in this study as they  
526 have been validated through various applications (Wang et al., 2014). Five Borg runs with  
527 different random number seeds were applied to each case study, and the results showed that  
528 the final optimization results were overall similar across different runs. Therefore, the results  
529 of a typical Borg run were presented to enable discussions for each of the two FSS case  
530 studies.

## 531 **4. Results and discussions**

### 532 **4.1 Calibration results of WDS nodal water consumptions**

533 For each FSS case study, nodal water consumptions of its associated WDS need to be  
534 calibrated at each time period, resulting in a total of 816 calibration runs using the calibration  
535 method as described in Section 2.3. The resultant time consumption was approximately 25  
536 seconds and 10 minutes for WDS-BKN and WDS-XZN systems, respectively, on a PC with a  
537 2.60-GHz Intel Core i9-7980XE and 2 GB of RAM. Fig. 7 shows the density plot of the  
538 errors between observations and simulations at the monitoring locations for both case studies. It  
539 is seen that, for the WDS-BKN case, more than 90% of the absolute errors (*AEs*) is less than  
540 0.30m for each pressure monitoring point (including the H2 sensor used for model validation),  
541 with the maximum *AE* being 0.32m across the three pressure monitoring points. In terms of

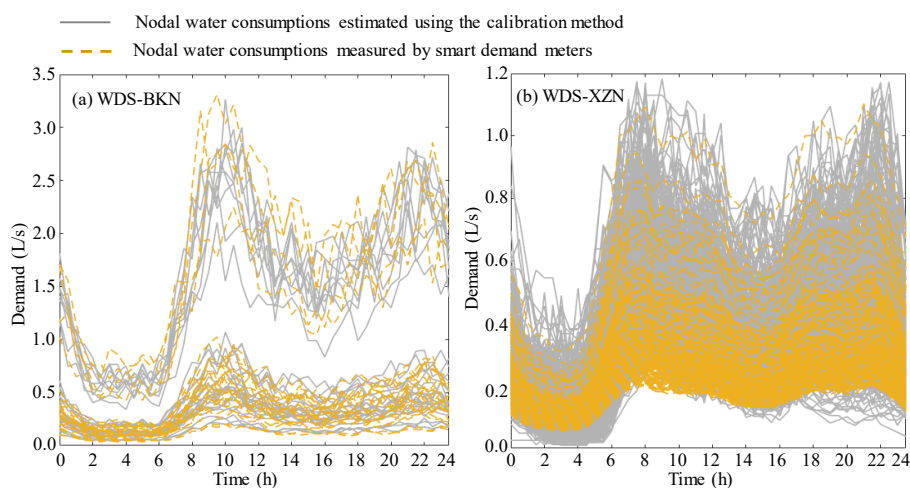
542 flow, more about 93% of absolute percentage errors (*APEs*) are smaller than 1.5%, with the  
 543 maximum *APE* being 2.40% as shown in Fig. 7(a, b). For the WDS-XZN (Fig. 7(c, d)), the  
 544 differences between the simulated and observed pressure values at the eight monitoring  
 545 locations are negligible (including H2, H5 and H7 used for validation), with all *AEs* being  
 546 lower than 0.4m. Relative to pressure, the deviations between the flow simulations and  
 547 observations are slightly larger (Figure 7(d)), with the majority of *APEs* smaller than 5% and  
 548 the maximum *APE* being 9.8% (F1 used for validation).



549  
 550 **Fig. 7 The probability density distribution of the errors between observations and**  
 551 **simulations for all monitoring locations of the WDS-BKN and WDS-XZN**



552 To further demonstrate the quality of calibration results, the criteria defined in Walski et al.  
 553 (2003) were used to verify the simulation accuracies. As stated in Walski et al. (2003), a  
 554 satisfactory WDS model calibration should ensure 85% of pressure errors within  $\pm 0.2\text{m}$ , 100%  
 555 of pressure errors within  $\pm 0.5\text{ m}$ , trunk main flow errors (flows more than 10% of the total  
 556 demands) within  $\pm 5\%$ , and the other flow errors within  $\pm 10\%$ . The calibration results of the  
 557 two WDSs satisfied these criteria, implying that the calibration was successful as the resultant  
 558 nodal water consumptions can reproduce the overall hydraulics of the WDS. Figure 8 presents  
 559 the nodal water consumptions over the 31 days with a resolution of 30-minute for the two  
 560 WDSs ((a) for the WDS-BKN and (b) for WDS-XZN), where the grey solid lines represent the  
 561 calibrated nodal water consumptions and the orange dotted lines indicate the nodal water  
 562 consumptions measured by smart demand meters. Despite some variations, all the nodal water  
 563 consumptions exhibited an overall similar trend for both WDSs, with two peak demand periods  
 564 occurring at each demand node as shown in Fig. 8, which matches well with the typical water  
 565 use properties (Zhang et al., 2018).



566

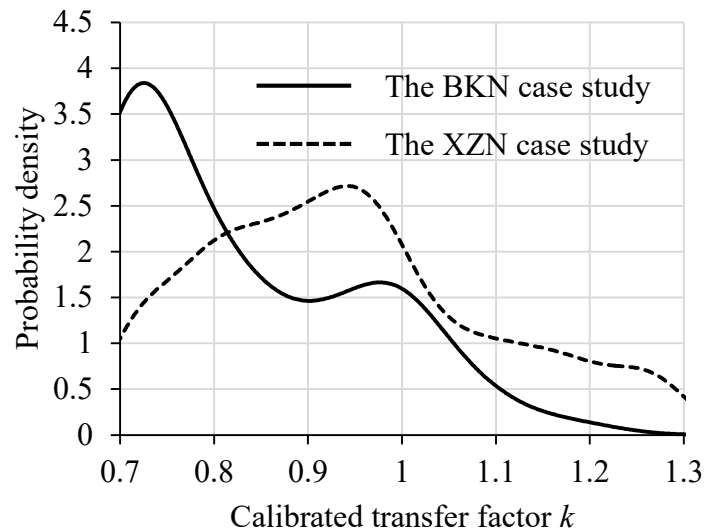
567 **Fig. 8 Nodal water consumptions of the two WDSs at a typical day with a 30-min time**

568

**resolution**

569 **4.2 Estimated transfer factor values**

570 Figure 9 shows the distribution of the probability density of the identified transfer factor  $k$   
571 values for all manholes of the BKN and XZN based on the historical data over the first 17  
572 calibration days (observations of the first three days were used as model setting-up). Such an  
573 optimization (Section 2.4) took 4.86 and 56 hours respectively based on the same computing  
574 platform as mentioned above. It can be seen that the majority of  $k$  values is within the range  
575 of 0.7~1.0 for the BKN and XZN, with a mean value of 0.83 and 0.92 respectively, meaning  
576 that around 83% and 92% of the total water consumptions have been collected by the FSS of  
577 BKN and XZN in this area, respectively. This demonstrates that the calibrated  $k$  values for all  
578 manholes were overall practically meaningful (Behzadian and Kapelan, 2015).



579

580 **Fig. 9 The density probability distribution of the identified transfer factor  $k$  for the BKN**  
581 **and XZN case study**

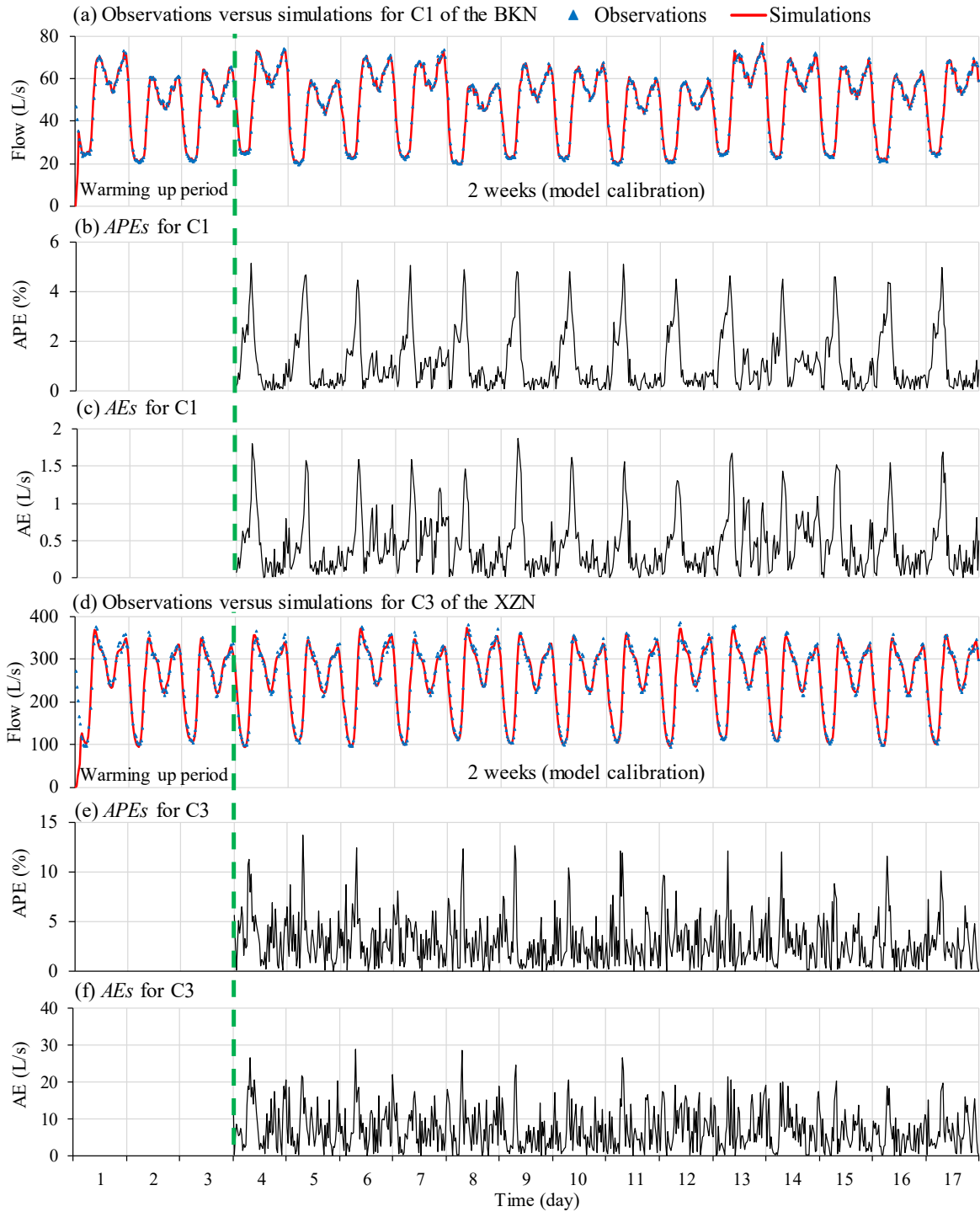
582 It is noted that around 10% and 28% calibrated  $k$  values were greater than 1 as shown in  
583 Figure 1. Such values were only allowed for the WDS nodes without smart demand sensors,  
584 and hence their nodal water consumptions were estimated using the calibration method

585 described in Section 2.3. While Fig. 7 showed that the calibration results can reproduce the  
586 overall hydraulics of the WDS at the monitoring locations, the calibrated nodal water  
587 consumptions might inevitably deviate from the true values at a certain extent (Zhang et al.,  
588 2018). To mitigate this potential impact, the value of  $k$  for the FSS manholes associated with  
589 WDS nodes without smart demand meters was allowed to have a range between 0.7 and 1.3,  
590 as previously stated. This led to that a proportion of  $k$  values were greater than 1 as shown in  
591 Fig. 9.

592 Fig. 10 shows the FSS calibrated results (the first 17 days) corresponding to the transfer factor  
593 values presented in Figure 9. It is seen that the simulated flows in C1 in the small BKN case  
594 study matched well with the observations (Fig. 10(a)), where all  $APE$  values were lower than  
595 5.0% and the mean  $APE$  value was 1.16%. For the XZN case study (Fig. 10(e)), the maximum  
596 and the mean  $APE$  values between simulations and observations within the calibration period  
597 at the C3 monitoring location were 13.68% and 3.02% respectively. Therefore, it can be  
598 deduced that the simulations matched well with the observations for such a large XZN case  
599 study. While the  $APE$  values at the period with relatively low sewer flows were relatively large,  
600 their corresponding absolute errors ( $AEs$ ) were overall low as shown in Figure 10 (c,f). For  
601 example, the maximum  $AE$  value was 1.88 L/s for the BKN case study with an average flow of  
602 48.47 L/s in C1 (Fig. 10(c)). Similarly, the maximum  $AE$  value was 30.51 L/s for the XZN case  
603 study with an average flow of 255.10 L/s in C3 (Fig.10(f)).

604 Tables 1 and 2 present the values of the performance metrics applied to the simulations and  
605 observations at monitoring locations for both case studies. As shown in this table, for the BKN

606 case study, the averaged values of *MAPE*,  $R^2$ , *NSE* and *KGE* over four different monitoring  
607 locations within the calibration period are 3.61%, 0.99, 0.94 and 0.94 respectively. For the large  
608 XZN case study, the averaged values of *MAPE*,  $R^2$ , *NSE* and *KGE* over 11 different monitoring  
609 locations within the calibration period are 4.98%, 0.98, 0.89 and 0.93 respectively. This implied  
610 that FSS calibration (aimed to estimate the transfer factor) was overall successful.



611

612

**Fig. 10 Observations versus simulations, as well as the APE (%) and AE(L/s) values for**

613

**C1 in the BKN, and C3 in the XZN within the calibration period (the first 17 days), where**

614

**C1 and C3 are shown in Fig. 4 and 5 respectively**

615

616 **Table 1 Values of the performance metrics applied to the simulations and observations**

617 **within the validation period for the BKN case study**

Sensor ID	Calibration period				Validation period			
	<i>MAPE</i> (%)	<i>R</i> <sup>2</sup>	<i>NSE</i>	<i>KGE</i>	<i>MAPE</i>	<i>R</i> <sup>2</sup>	<i>NSE</i>	<i>KGE</i>
M1	3.18	0.99	0.97	0.93	3.20	0.99	0.96	0.93
M2	2.06	0.99	0.97	0.93	2.12	0.99	0.97	0.92
M3	8.05	0.99	0.84	0.89	8.04	0.99	0.84	0.88
C1	1.16	0.99	0.99	0.99	1.15	0.99	0.99	0.98
<b>Average</b>	<b>3.61</b>	<b>0.99</b>	<b>0.94</b>	<b>0.94</b>	<b>3.63</b>	<b>0.99</b>	<b>0.94</b>	<b>0.93</b>

618 **Table 2 Values of the performance metrics applied to the simulations and observations**

619 **within the validation period for the XZN case study**

Sensor ID	Calibration period				Validation period			
	<i>MAPE</i> (%)	<i>R</i> <sup>2</sup>	<i>NSE</i>	<i>KGE</i>	<i>MAPE</i> (%)	<i>R</i> <sup>2</sup>	<i>NSE</i>	<i>KGE</i>
M1	7.85	0.98	0.78	0.87	7.79	0.97	0.77	0.87
M2	6.49	0.97	0.83	0.90	6.81	0.96	0.80	0.88
M3	6.82	0.98	0.81	0.89	6.43	0.96	0.81	0.89
M4	8.09	0.98	0.77	0.87	8.08	0.97	0.77	0.87
M5	2.83	0.98	0.95	0.96	3.33	0.96	0.94	0.96
M6	7.09	0.97	0.79	0.89	7.07	0.96	0.79	0.88
M7	3.56	0.98	0.93	0.91	4.23	0.96	0.91	0.91
M8	3.10	0.97	0.95	0.92	3.45	0.96	0.94	0.91
C1	2.89	0.99	0.99	0.99	3.20	0.99	0.99	0.99
C2	3.00	0.99	0.99	0.99	3.57	0.98	0.98	0.99
C3	3.02	0.99	0.99	0.99	3.62	0.98	0.98	0.99
<b>Average</b>	<b>4.98</b>	<b>0.98</b>	<b>0.89</b>	<b>0.93</b>	<b>5.23</b>	<b>0.97</b>	<b>0.88</b>	<b>0.92</b>

620 **4.3 Performance of the real-time FSS modelling**

621 Results in the calibration period demonstrated that the proposed method was capable of

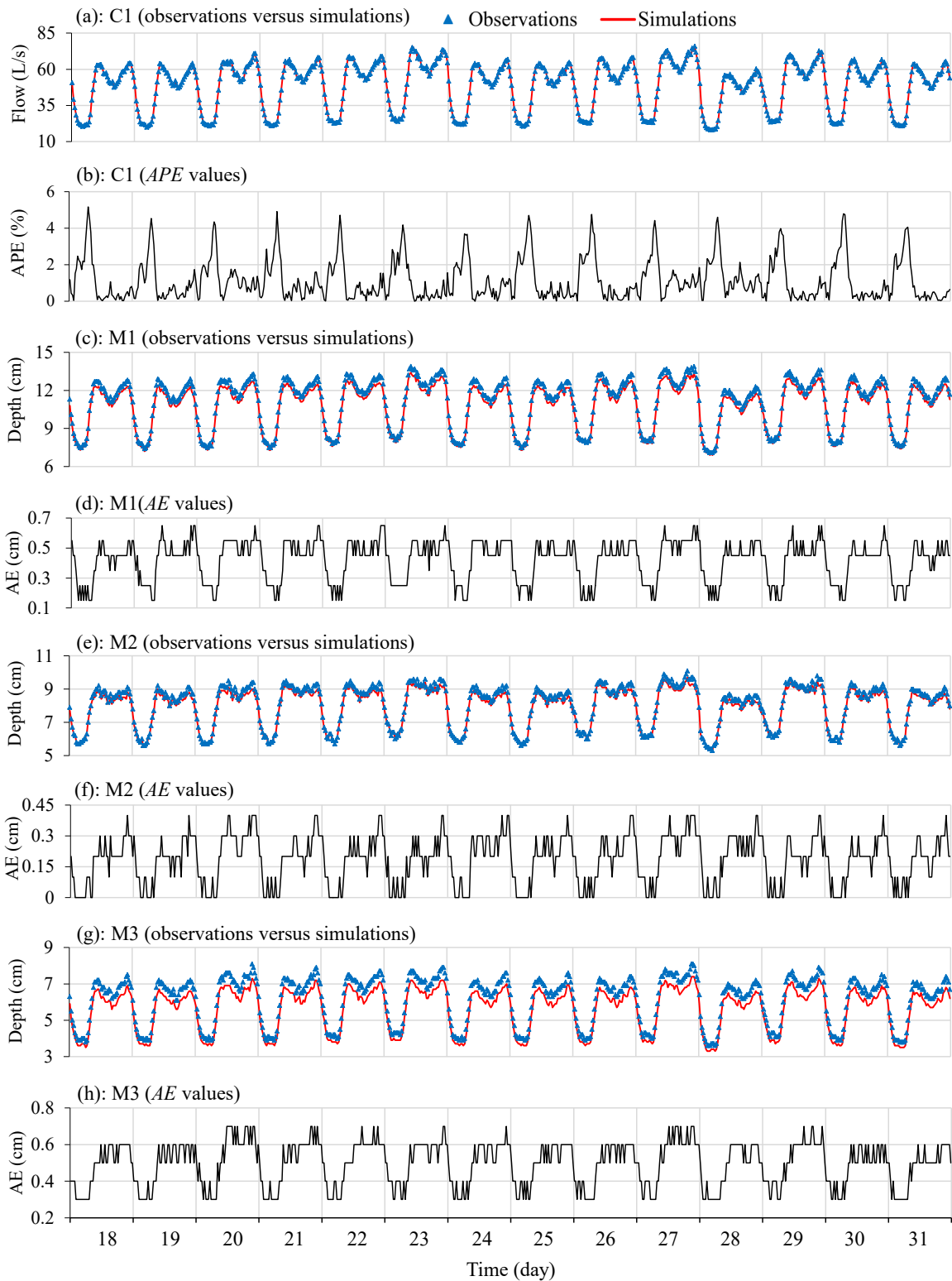
622 identifying suitable transfer factors that can match well simulations and observations at the

623 monitoring locations. This section validated the performance of the real-time FSS models

624 driven by the WDS consumption data in modelling the sewer hydraulics and such a

625 performance evaluation was conducted using the observations from the 17<sup>th</sup> to the 31<sup>st</sup> days (i.e.,  
626 validation period). The steps of the real-time FSS modelling were presented in Figure 2  
627 (real-time module). Figures 11 and 12 show the observations versus observations of the  
628 monitoring locations every 30 minutes within the validation period for both case studies.

629 It is seen from Figure 11 that the sewer flow and the water depth simulations matched well with  
630 the observations within the validation period at the four monitoring locations (C1, M1, M2 and  
631 M3) in the BKN case study. More specifically, the maximum flow *APE* value was 4.91%, and  
632 the maximum absolute error of water depth was 0.7 cm across M1, M2 and M3 locations.  
633 Similarly, the differences between the simulation and observations for C1, C2, M1 and M5  
634 monitoring locations were also matched very well for the XZN case study as shown in Fig.  
635 12. For this large FSS, the maximum flow *APE* value was 13.45% and the maximum absolute  
636 error of water depth was 1.4 cm (similar observations can be made for other monitoring  
637 locations).



638

639

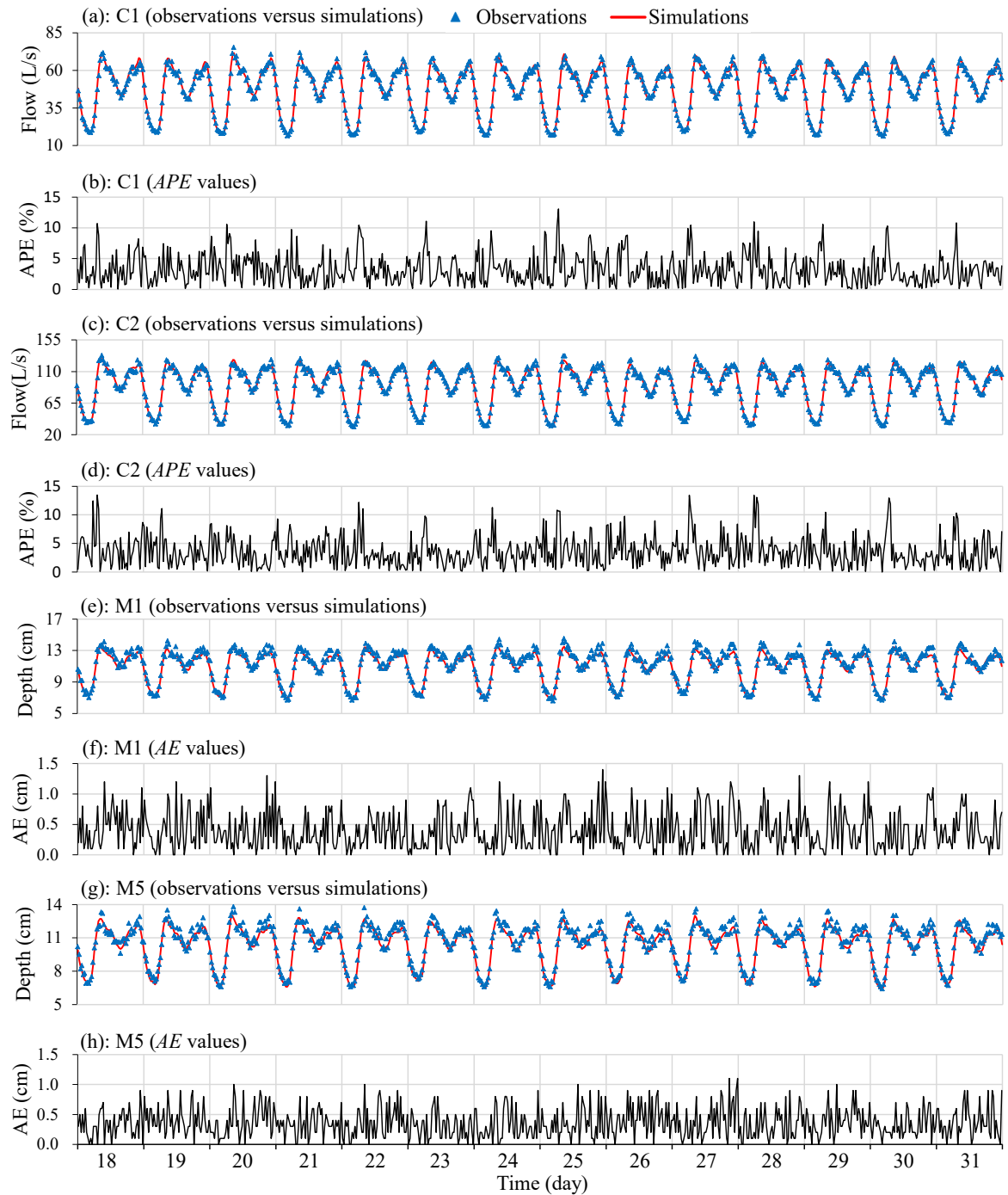
**Fig. 11 Observations versus simulations, as well as the APEs or AEs for the four**

640

**monitoring locations (shown in Fig. 4) within the validation period of the BKN case study**

641





642

643 **Fig. 12 Observations versus simulations, as well as the APEs or AEs for the four**

644 **monitoring locations (shown in Fig. 5) within the validation period of the XZN case study**

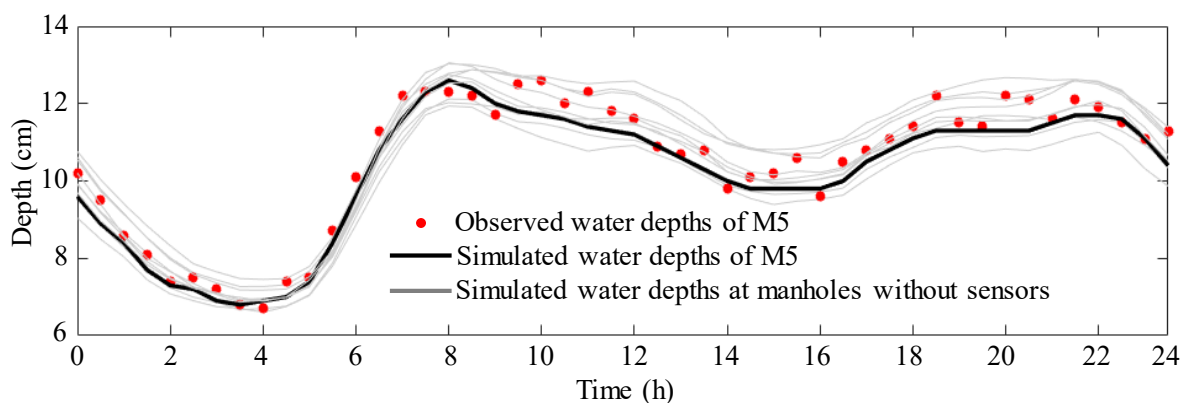
645 The values of performance metrics applied to the observations and simulations within the

646 validation period for both case studies are also presented in Tables 1 and 2 respectively. As

647 shown in these two tables, the averaged values of *MAPE*,  $R^2$ , *NSE* and *KGE* over four different  
648 monitoring locations within the validation period are 3.63%, 0.99, 0.94 and 0.93 respectively  
649 for the BKN case study. The averaged values of *MAPE*,  $R^2$ , *NSE* and *KGE* over four different  
650 monitoring locations within the validation period are 5.23%, 0.97, 0.88 and 0.92 respectively  
651 for the XZN case study. Overall, the performance of the FSS models within the validation  
652 period was similar or slightly worse than the calibration period for both case studies (see Tables  
653 1 and 2). This indicated that (i) there was a low likelihood of over-fitting within the calibration  
654 process due to the similar performance between the calibration and validation period, and (ii)  
655 the real-time FSS models driven by WDS water consumption data were effective in accurately  
656 simulating the sewer hydraulics at a high time resolution (very 30 minutes).

657 The real-time model was able to offer a great opportunity to enable the comparison between the  
658 simulations and observations at monitoring locations at a very high time resolution (every 30  
659 minutes in this paper), followed by a warning trigger if large deviations between the  
660 simulations and observations were observed. More specifically, a threshold can be determined  
661 by long-term historical data for each monitoring location as did in Qi et al. (2018). If the  
662 deviations between the simulations and observations at a particular monitoring location go  
663 beyond the specified range, a warning can be triggered efficiently. It should be highlighted that  
664 since the real-time FSS model developed using the proposed method has already accounted for  
665 the inflow variation caused by the change in water consumption, the false warning rate is  
666 expected to be significantly reduced. Therefore, the proposed real-time FSS model can be a  
667 useful tool for the development of an efficient warning system, aimed to detect the potential  
668 hydraulic issues (e.g., leaks and illicit inflows) for the FSSs.

669 In addition to providing accurate simulations at the monitoring locations, the proposed method  
670 was also able to produce real-time simulations for the manholes and sewer pipes without  
671 monitoring sensors. While the accuracies of these simulations cannot be directly evaluated due  
672 to the unavailability of observations, it can be anticipated that they can reasonably represent the  
673 true hydraulics of the manholes and sewer pipes without monitoring sensors. This was because  
674 the real-time FSS model was driven by the water consumption data from the water distribution  
675 system, where nodal water consumptions were either measured by smart demand meters or  
676 estimated with the aid of an intensive sensor (pressure and flow sensors) coverage. As shown in  
677 Figure 13, water depths of 10 manholes near M5 sensor of the XZN case study over a typical  
678 day within the validation period exhibited a similar and reasonable trend. These accurate  
679 hydraulic simulations at the manholes and pipes without monitoring sensors can be useful to  
680 enable the efficient localization of leaks, deposits or illicit inflows, through comparing the  
681 simulations with the sampled observations from the field survey.



682

683 **Fig. 13 Water depth simulations and observations of M5, as well as the water depth**  
684 **simulations of 10 manholes near M5 without sensors in the XZN case study in 18<sup>th</sup> day**  
685 **within the validation period**

## 686 5. Conclusions

687 This paper proposes a novel method to develop a real-time foul sewer system (FSS) model  
688 driven by water consumption data from its associated water distribution system (WDS) that  
689 often has a large number of sensors such as pressure sensors, flow meters and smart demand  
690 meters. Within the proposed method, the FSS and the WDS models are integrated to build  
691 physical connections between water consumption nodes and their corresponding manholes  
692 based on spatial distances. This is followed by a proposal of an optimization approach to  
693 identify the transfer factor  $k$  between nodal water consumptions and FSS manhole inflows  
694 according to historical observations. Subsequently, real-time nodal water consumption data  
695 are acquired using an efficient calibration approach based on the dense sensors in the WDS.  
696 Finally, these nodal water consumption data combined with the identified  $k$  values drive the  
697 FSS real-time modelling.

698 Two real FSS case studies, the smaller BKN with 64 sewer pipes and 64 manholes and the large  
699 ZXN case study with 1214 sewer pipes and 1214 manholes have been used to test/validate and  
700 demonstrate the proposed method. The results obtained demonstrate that the proposed method  
701 can produce real-time predictions of water depths and flows that are in good agreements with  
702 the corresponding observations at monitoring locations. The evidence for this can be found in  
703 the high mean values of  $R^2$ ,  $NSE$  and  $KGE$  metrics obtained across different monitoring  
704 locations, which are 0.99, 0.94 and 0.93 of the small BNK case study, and 0.97, 0.88 and 0.92  
705 for the large XZN case study, respectively. In addition to providing accurate simulations at the  
706 monitoring locations, the proposed method is expected to produce reasonable real-time

707 simulations for the manholes and sewer pipes without monitoring sensors. This deduction is  
708 based on that the real-time FSS model is driven by the WDS water consumption data that are  
709 either measured by smart demand meters or estimated based on a large number of sensors  
710 (pressure and flow sensors). This implies that the “equifinality” problem can be successfully  
711 addressed by using the proposed method. Therefore, the developed real-time FSS model offers  
712 an important tool to facilitate effective and efficient foul sewer system management and  
713 operation.

714 Finally, it is acknowledged that the proposed method is developed ignoring a number of  
715 uncertainties that exist in reality. These include potential inaccuracies of WDS and FSS sensor  
716 measurements (e.g., smart demand meters, water depth sensors, flow sensors), the potential  
717 impacts of the ignorance of the water travelling time within the user property and the influence  
718 of the variation in Manning’s coefficients of the sewer pipes. These uncertainties need to be  
719 more systematically investigated in a future study.

## 720 **Acknowledgement**

721 This work is funded by the National Natural Science Foundation of China (Grant No.  
722 51922096), and the Excellent Youth Natural Science Foundation of Zhejiang Province, China  
723 (LR19E080003).

## 724 **References**

725 Ahm, M., Thorndahl, S., Nielsen, J.E. and Rasmussen, M.R. (2016) Estimation of combined  
726 sewer overflow discharge: a software sensor approach based on local water level  
727 measurements. *Water Science and Technology* 74(11), 2683-2696.

728 Bailey, O., Arnot, T.C., Blokker, E.J.M., Kapelan, Z., Vreeburg, J. and Hofman, J. (2019)  
729 Developing a stochastic sewer model to support sewer design under water conservation  
730 measures. *Journal of Hydrology* 573, 908-917.

731 Banik, B.K., Di Cristo, C., Leopardi, A. and de Marinis, G. (2017) Illicit intrusion  
732 characterization in sewer systems. *Urban Water Journal* 14(4), 416-426.

733 Beheshti, M. and Saegrov, S. (2019) Detection of extraneous water ingress into the sewer  
734 system using tandem methods - a case study in Trondheim city. *Water Science and*  
735 *Technology* 79(2), 231-239.

736 Behzadian, K. and Kapelan, Z. (2015) Modelling metabolism based performance of an urban  
737 water system using WaterMet(2). *Resources Conservation and Recycling* 99, 84-99.

738 Behzadian, K., Kapelan, Z., Venkatesh, G., Brattebø, H. and Sægrov, S. (2014) WaterMet2: A  
739 tool for integrated analysis of sustainability-based performance of urban water systems.  
740 *Drinking Water Engineering Sciences* 7, 63-72.

741 Black, J. and Endreny, T. (2006) Increasing stormwater outfall duration, magnitude, and  
742 volume through combined sewer separation. *Journal of Hydrologic Engineering* 11(5),  
743 472-481.

744 Breinholt, A., Grum, M., Madsen, H., Thordarson, F.O. and Mikkelsen, P.S. (2013) Informal  
745 uncertainty analysis (GLUE) of continuous flow simulation in a hybrid sewer system  
746 with infiltration inflow - consistency of containment ratios in calibration and validation?  
747 *Hydrology and Earth System Sciences* 17(10), 4159-4176.

748 Broekhuizen, I., Leonhardt, G., Marsalek, J. and Viklander, M. (2020) Event selection and  
749 two-stage approach for calibrating models of green urban drainage systems. *Hydrology*

750 and Earth System Sciences 24(2), 869-885.

751 Bruen, M. and Yang, J.Q. (2006) Combined hydraulic and black-box models for flood  
752 forecasting in urban drainage systems. Journal of Hydrologic Engineering 11(6),  
753 589-596.

754 Burke, C., Molzahn, R., Pherson, P. and Coutts, P. (1986) An evaluation of a sanitary sewer  
755 system using a computer model. Tunnelling and Underground Space Technology -  
756 TUNN UNDERGR SPACE TECHNOL 1, 153-161.

757 Creaco, E., Campisano, A., Fontana, N., Marini, G., Page, P.R. and Walski, T. (2019) Real  
758 time control of water distribution networks: A state-of-the-art review. Water Research  
759 161, 517-530.

760 Creaco, E., Signori, P., Papiri, S. and Ciaponi, C. (2018) Peak Demand Assessment and  
761 Hydraulic Analysis in WDN Design. Journal of Water Resources Planning and  
762 Management 144(6).

763 Di Pierro, A., Hankin, C. and Wiklicky, H. (2005) Quantitative static analysis of distributed  
764 systems. Journal of Functional Programming 15, 703-749.

765 Du, K., Long, T.-Y., Wang, J.-H. and Guo, J.-S. (2015) Inversion Model of Water Distribution  
766 Systems for Nodal Demand Calibration. Journal of Water Resources Planning and  
767 Management 141(9).

768 Eren, B. and Karadagli, F. (2012) Physical Disintegration of Toilet Papers in Wastewater  
769 Systems: Experimental Analysis and Mathematical Modeling. Environmental Science &  
770 Technology 46(5), 2870-2876.

771 Garda, A., Castillo, F., Binet, G., Litrico, X. and Gil, A. (2016) Needs and potential of

772 unmanned vehicles in sewers. *Houille Blanche-Revue Internationale De L Eau* (1),  
773 24-29.

774 Gujarati, D.N. (2009) *Basic econometrics*. Tata McGraw-Hill Education.

775 Guo, D., Zheng, F., Gupta, H. and Maier, H.R. (2020) On the Robustness of Conceptual  
776 Rainfall-Runoff Models to Calibration and Evaluation Data Set Splits Selection: A Large  
777 Sample Investigation. *Water Resources Research* 56(3).

778 Hadka, D. and Reed, P. (2013) Borg: An Auto-Adaptive Many-Objective Evolutionary  
779 Computing Framework. *Evolutionary Computation* 21(2), 231-259.

780 He, G., Zhang, T., Zheng, F. and Zhang, Q. (2018) An efficient multi-objective optimization  
781 method for water quality sensor placement within water distribution systems considering  
782 contamination probability variations. *Water Research* 143, 165-175.

783 Huang, D., Liu, X.H., Jiang, S.Z., Wang, H.C., Wang, J.Y. and Zhang, Y.K. (2018) Current  
784 state and future perspectives of sewer networks in urban China. *Frontiers of*  
785 *Environmental Science & Engineering* 12(3), 16.

786 Huang, Y., Zheng, F., Duan, H.-F., Zhang, T., Guo, X. and Zhang, Q. (2019) Skeletonizing  
787 Pipes in Series within Urban Water Distribution Systems Using a Transient-Based  
788 Method. *Journal of Hydraulic Engineering* 145(2).

789 Irvine, K., Maryc, R., Vermette, S., Bakert, J. and Kleinfelder, K. (2011) Illicit discharge  
790 detection and elimination: Low cost options for source identification and trackdown in  
791 stormwater systems. *Urban Water Journal* 8(6), 379-395.

792 Joseph-Duran, B., Ocampo-Martinez, C. and Cembrano, G. (2014) Hybrid modeling and  
793 receding horizon control of sewer networks. *Water Resources Research* 50(11),



794 8497-8514.

795 Kapelan, Z. (2002) Calibration of water distribution system hydraulic models.

796 Khu, S.T., di Pierro, F., Savic, D., Djordjevic, S. and Walters, G.A. (2006) Incorporating  
797 spatial and temporal information for urban drainage model calibration: An approach  
798 using preference ordering genetic algorithm. *Advances in Water Resources* 29(8),  
799 1168-1181.

800 Kleidorfer, M., Leonhardt, G. and Rauch, W. (2012) Identifiability analysis in conceptual  
801 sewer modelling. *Water Science and Technology* 66(7), 1467-1474.

802 Knobens, W.J.M., Freer, J.E. and Woods, R.A. (2019) Technical note: Inherent benchmark or  
803 not? Comparing Nash-Sutcliffe and Kling-Gupta efficiency scores. *Hydrology and Earth  
804 System Sciences* 23(10), 4323-4331.

805 Koch, M.W. and McKenna, S.A. (2011) Distributed Sensor Fusion in Water Quality Event  
806 Detection. *Journal of Water Resources Planning and Management* 137(1), 10-19.

807 Korving, H. and Clemens, F. (2005) Impact of dimension uncertainty and model calibration  
808 on sewer system assessment. *Water Science and Technology* 52(5), 35-42.

809 Lepot, M., Makris, K.F. and Clemens, F. (2017) Detection and quantification of lateral, illicit  
810 connections and infiltration in sewers with Infra-Red camera: Conclusions after a wide  
811 experimental plan. *Water Research* 122, 678-691.

812 Li, T., Zhang, W., Feng, C. and Shen, J. (2014) Performance assessment of separate and  
813 combined sewer systems in metropolitan areas in southern China. *Water Science and  
814 Technology* 69(2), 422-429.

815 Lim, J.S., Kim, J., Friedman, J., Lee, U., Vieira, L., Rosso, D., Gerla, M. and Srivastava, M.B.

816 (2013) SewerSnort: A drifting sensor for in situ Wastewater Collection System gas  
817 monitoring. *Ad Hoc Networks* 11(4), 1456-1471.

818 Liu, Y., Tugtas, A.E., Sharma, K.R., Ni, B.-J. and Yuan, Z. (2016) Sulfide and methane  
819 production in sewer sediments: Field survey and model evaluation. *Water Research* 89,  
820 142-150.

821 McCall, A.-K., Bade, R., Kinyua, J., Lai, F.Y., Thai, P.K., Covaci, A., Bijlsma, L., van Nuijs,  
822 A.L.N. and Ort, C. (2016) Critical review on the stability of illicit drugs in sewers and  
823 wastewater samples. *Water Research* 88, 933-947.

824 Mu, L., Zheng, F., Tao, R., Zhang, Q. and Kapelan, Z. (2020) Hourly and Daily Urban Water  
825 Demand Predictions Using a Long Short-Term Memory Based Model. *Journal of Water  
826 Resources Planning and Management* 146(9).

827 Nash, J.E. and Sutcliffe, J. (1970) River Flow Forecasting Through Conceptual Models: Part  
828 1. — A Discussion of Principles. *Journal of Hydrology* 10, 282.

829 Qi, Z., Zheng, F., Guo, D., Maier, H.R., Zhang, T., Yu, T. and Shao, Y. (2018) Better  
830 Understanding of the Capacity of Pressure Sensor Systems to Detect Pipe Burst within  
831 Water Distribution Networks. *Journal of Water Resources Planning and Management*  
832 144(7).

833 Rauch, W., Bertrand-Krajewski, J. L., Krebs, P., Mark, O., Schilling, W., Schütze, M., and  
834 Vanrolleghem, P. A. (2001). Mathematical modelling of integrated urban drainage  
835 systems. Keynote paper. In *Second International Conference on Interactions between  
836 sewers, treatment plants and receiving waters-INTERURBA II, Lisbon/Portugal*, 89-106.

837 Reed, P.M., Hadka, D., Herman, J.D., Kasprzyk, J.R. and Kollat, J.B. (2013) Evolutionary

838 multiobjective optimization in water resources: The past, present, and future. *Advances*  
839 *in Water Resources* 51, 438-456.

840 Rokstad, M.M. and Ugarelli, R.M. (2015) Evaluating the role of deterioration models for  
841 condition assessment of sewers. *Journal of Hydroinformatics* 17(5), 789-804.

842 Rossman, L.A. (2000) users manual. National Risk Management Research Laboratory.

843 Rossman, L.A. (2010) Storm Water Management Model User's Manual.

844 Rossman, L.A. and Huber, W. (2017) Storm water management model reference manual  
845 volume II—hydraulics. US Environmental Protection Agency, 190.

846 Sambito, M., Di Cristo, C., Freni, G. and Leopardi, A. (2020) Optimal water quality sensor  
847 positioning in urban drainage systems for illicit intrusion identification. *Journal of*  
848 *Hydroinformatics* 22(1), 46-60.

849 Sara C. Troutman, Nancy G. Love, Branko Kerkez. (2020) Balancing water quality and flows  
850 in combined sewer systems using real-time control. *Environmental Science: Water*  
851 *Research & Technology* 6 (5), pages 1357-1369.

852 Savic, D.A., Kapelan, Z.S. and Jonkergouw, P.M.R. (2009) Quo vadis water distribution  
853 model calibration? *Urban Water Journal* 6(1), 3-22.

854 Schilperoort, R., Hoppe, H., de Haan, C. and Langeveld, J. (2013) Searching for storm water  
855 inflows in foul sewers using fibre-optic distributed temperature sensing. *Water Science*  
856 *and Technology* 68(8), 1723-1730.

857 Schütze M, Campisano A, Colas H, Schilling W and Vanrolleghem, P. A. (2002). Real-time  
858 control of urban wastewater systems-where do we stand today? *Global Solutions for*  
859 *Urban Drainage*, 1-17.

860 Schütze, M., Campisano, A., Colas, H., Vanrolleghem, P., and Schilling, W. (2003). Real-time  
861 control of urban water systems. In International Conference on Pumps,  
862 Electromechanical Devices and Systems Applied to Urban Water Management PEDS,  
863 22-25.

864 Seco, I., Schellart, A., Gomez-Valentin, M. and Tait, S. (2018) Prediction of Organic  
865 Combined Sewer Sediment Release and Transport. Journal of Hydraulic Engineering  
866 144(3).

867 Sweetapple, C., Astaraie-Imani, M. and Butler, D. (2018) Design and operation of urban  
868 wastewater systems considering reliability, risk and resilience. Water Research 147,  
869 1-12.

870 Talaiekhosani, A., Bagheri, M., Goli, A. and Khoozani, M.R.T. (2016) An overview of  
871 principles of odor production, emission, and control methods in wastewater collection  
872 and treatment systems. Journal of Environmental Management 170, 186-206.

873 Walski, T.M., Chase, D.V., Savic, D.A., Grayman, W., Beckwith, S. and Koelle, E. (2003)  
874 Advanced water distribution modeling and management.

875 Wang, Q., Guidolin, M., Savic, D. and Kapelan, Z. (2015) Two-Objective Design of  
876 Benchmark Problems of a Water Distribution System via MOEAs: Towards the  
877 Best-Known Approximation of the True Pareto Front. Journal of Water Resources  
878 Planning and Management 141(3).

879 Wu, Z.Y., Farley, M., Turtle, D., Kapelan, Z., Boxall, J., Mounce, S., Dahasahasra, S., Mulay,  
880 M. and Kleiner, Y. (2011) Water loss reduction, Bentley Institute Press.

881 Wu, Z.Y., Sage, P. and Turtle, D. (2010) Pressure-Dependent Leak Detection Model and Its

882 Application to a District Water System. *Journal of Water Resources Planning and*  
883 *Management* 136(1), 116-128.

884 Xie, X., Zhang, H. and Hou, D. (2017) Bayesian Approach for Joint Estimation of Demand  
885 and Roughness in Water Distribution Systems. *Journal of Water Resources Planning and*  
886 *Management* 143(8).

887 Zhang, Q., Zheng, F., Duan, H.-F., Jia, Y., Zhang, T. and Guo, X. (2018) Efficient Numerical  
888 Approach for Simultaneous Calibration of Pipe Roughness Coefficients and Nodal  
889 Demands for Water Distribution Systems. *Journal of Water Resources Planning and*  
890 *Management* 144(10).

891 Zheng, F., Tao, R., Maier, H.R., See, L., Savic, D., Zhang, T., Chen, Q., Assumpcao, T.H.,  
892 Yang, P., Heidari, B., Rieckermann, J., Minsker, B., Bi, W., Cai, X., Solomatine, D. and  
893 Popescu, I. (2018) Crowdsourcing Methods for Data Collection in Geophysics: State of  
894 the Art, Issues, and Future Directions. *Reviews of Geophysics* 56(4), 698-740.

895 Zheng, F., Zecchin, A.C., Maier, H.R. and Simpson, A.R. (2016) Comparison of the  
896 Searching Behavior of NSGA-II, SAMODE, and Borg MOEAs Applied to Water  
897 Distribution System Design Problems. *Journal of Water Resources Planning and*  
898 *Management* 142(7).

899 Zheng, F., Zecchin, A.C., Newman, J.P., Maier, H.R. and Dandy, G.C. (2017) An Adaptive  
900 Convergence-Trajectory Controlled Ant Colony Optimization Algorithm With  
901 Application to Water Distribution System Design Problems. *Ieee Transactions on*  
902 *Evolutionary Computation* 21(5), 773-791.